

# Explosion Models for Type Ia Supernovae: A comparison with observed light curves, distances, $H_0$ and $q_0$

P. Höflich<sup>1</sup> and A. Khokhlov<sup>2</sup>

1. Center for Astrophysics, Harvard University, 60 Garden Street, Cambridge, MA 02138
2. Department of Astronomy, University of Texas, Austin, TX 07871

## Abstract

Theoretical monochromatic light curves and photospheric expansion velocities are compared with observations of 27 Type Ia supernovae (SNe Ia). A set of 37 models has been considered which encompasses all currently discussed explosion scenarios for Type Ia supernovae including deflagrations, detonations, delayed detonations, pulsating delayed detonations and tamped detonations of Chandrasekhar mass, and Helium detonations of low mass white dwarfs. The explosions are calculated using one-dimensional Lagrangian hydro and radiation-hydro codes with incorporated nuclear networks. Subsequently, light curves are constructed using our LC scheme which includes an implicit radiation transport, expansion opacities, a Monte-Carlo  $\gamma$ -ray transport, and molecular and dust formation. For some supernovae, results of detailed non-LTE calculations have been considered.

Observational properties of our series of models are discussed, in particular, the relation between the absolute brightness, post-maximum decline rates, the colors at several moments of time, etc. All models with a  $^{56}\text{Ni}$  production larger than  $\approx 0.4M_{\odot}$  produce light curves of similar brightness. The influence of the cosmological red shift on the light curves and on the correction for interstellar reddening is discussed.

Based on data rectification of the standard deviation, a quantitative procedure to fit the observations has been used to determine the free parameters, i.e. the distance, the reddening, and the time of the explosion. Fast rising light curves (e.g., SN 1981B and SN 1994D) can be reproduced by delayed detonation models or deflagration models similar to W7. Slowly rising ( $t_{max} \geq 16$  days) light curves (e.g., SN 1984A and SN 1990N) cannot be reproduced by standard detonation, deflagration, or delayed detonation models. To obtain an acceptable agreement with observations, models are required where the C/O white dwarf is surrounded by an unburnt extended envelope of typically 0.2 to 0.4  $M_{\odot}$  which may either be pre-existing or produced during the explosion. Our interpretation of the light curves is also supported by the photospheric expansion velocities. Mainly due to the fast increase of the  $\gamma$  radiation produced by the outer  $^{56}\text{Ni}$ , the post maximum decline of Helium detonations tends to be faster compared to observations of normal bright SNe Ia.

Strongly subluminal SNe Ia can be understood in the framework of pulsating delayed detonations, both from the absolute brightness and the colors. Alternatively, subluminality can be produced within the scenario of helium detonations in low mass white dwarfs of about 0.6 to 0.8  $M_{\odot}$  if the explosion occurs when rather little Helium has been accreted. However, even subluminal Helium detonation models are very blue at maximum light owing to heating in the outer layers and brighter models show a fast postmaximum decline, in contradiction to the observations.

We find evidence for a correlation between the type of host galaxy and the explosion mechanism. In spiral galaxies, about the same amount of prompt explosions (delayed detonations and W7) and pulsating delayed detonations seems to occur. In contrast, in ellipticals, the latter type is strongly favored. This difference may provide a hint about the stellar evolution of the progenitors.

Based on a comparison of theoretical light curves and observational data, the distances of the parent galaxies are determined independent from secondary distance indicators. A comparison with theoretical models allows for a consistent determination of the interstellar reddening and the cosmological red shift. For the example of SN 1988U, we show the need for a simultaneous use of both spectral and light curve data if the data set is incomplete. Based on the models, SNe Ia allow for a measurement of the value of the Hubble constant  $H_0$ .  $H_0$  is found to be  $67 \pm 9 \text{ km}/(\text{secMpc})$  within a 95 % probability for distances up to 1.3 Gpc. SN1988U at 1.3 Gpc is consistent with a deceleration parameter  $q_0$  of  $0.7 \pm 0.5$ .

*Subject headings:* Supernovae and supernovae remnants: general – hydrodynamics – radiation transfer – light curves – Hubble constant – deceleration parameter  $q_0$

## 1. Introduction

Type Ia Supernovae (SNe Ia) may reach the same brightness as the entire parent galaxy. In principle, this allows for the measurements of extragalactic distances and cosmological parameters such as the Hubble constant  $H_0$  and the deceleration parameter  $q_0$ . However, the absolute brightness must be known either by using distance calibrators or theoretical models for the light curves and spectra. Type Ia events are major contributors to the production of heavy elements. An understanding of the underlying physics is important for our picture of the chemical evolution of galaxies. Improvements in the observations and theoretical calculations have resulted in the rapid growth of our knowledge of these objects, but have also raised several new questions on the explosion mechanism and the homogeneity of SNe Ia.

During the last two decades, the observational database for Type Ia supernovae has significantly increased. Both the similarity of their light curves and spectra favored the idea that SNe Ia form a homogeneous class and, thus, can be used as standard candles (for a recent review see Branch & Tammann 1992). However, several authors have raised doubts in the past about the homogeneity of SNe Ia and, nowadays, a spread in the properties of SNe Ia is widely accepted. Based on a large number of photometric light curves, Barbon, Ciatti & Rosino (1978) divided SNe Ia into “fast” and “slow” events depending on the rate of decline from maximum, the contrast from peak to tail, and the rate of decline of the tail. Pskovskii (1970, 1977) and Branch (1981) argued that SNe Ia form a continuous sequence, the expansion velocity and the peak absolute magnitude being correlated with the rate of decline from maximum. The  $B$  and  $V$  light curves of SN 1986G declined faster after maximum than those of SN 1981B (Phillips et al. 1987; Cristiani et al. 1992), the infrared light curve of SN 1986G was unusual (Frogel et al. 1987), the optical spectra of SN 1986G (Phillips et al. 1987) and of SN 1990N (Leibundgut et al. 1991) showed small but significant anomalies, and pre-maximum observations of SN 1991T exhibited large deviations from the “standard” behaviour of SNe Ia (Filippenko et al. 1992a; Phillips et al. 1992; Hamuy et al. 1995). Finally, the “unusual” Type Ia supernova SN 1991bg clearly proved the existence of a wide diversity among SNe Ia. Besides showing other peculiarities, SN1991bg was dimmer than SN 1957B, another SN Ia in the same galaxy, by  $\sim 2.5$  mag in  $B$  and by  $\sim 1.5$  mag in  $V$  (Filippenko et al. 1992ab; Leibundgut et al. 1993).

Despite all uncertainties, it is widely accepted that SNe Ia are thermonuclear explosions of carbon-oxygen white dwarfs (Hoyle & Fowler 1960; for discussions of various theoretical aspects see Woosley and Weaver 1986, 1995, Wheeler & Harkness 1990, Canal 1995, Nomoto et al. 1995, Nomoto 1995, and Wheeler et al. 1995). Three main scenarios can be distinguished.

A first group consists of massive carbon-oxygen white dwarfs (WDs) with a mass close to the Chandrasekhar mass which accrete mass through Roche-lobe overflow

from an evolved companion star (Nomoto & Sugimoto 1977; Nomoto 1982). In these accretion models, the explosion is triggered by compressional heating. From the theoretical standpoint, the key question is how the flame propagates through the white dwarf. Several models of Type Ia supernovae have been proposed in the past, including detonation (Arnett 1969; Hansen & Wheeler 1969), deflagration (Ivanova, Imshennik & Chechetkin 1974; Nomoto, Sugimoto & Neo 1976) and the delayed detonation model, which assumes that the flame starts as a deflagration and turns into a detonation later on (Khokhlov 1991ab, Woosley & Weaver 1995, Yamaoka et al. 1992).

The second group of progenitor models consists of two low-mass white dwarfs in a close orbit which decays due to the emission of gravitational radiation and this, eventually, leads to the merging of the two WDs. In an intermediate step, these models form a low density WD surrounded by a CO envelope (Webbink 1984; Iben & Tutukov 1984; Paczyński 1985).

Another class of models – double detonation of a C/O-WD triggered by detonation of helium layer in low-mass white dwarfs – was explored by Nomoto (1980), Woosley, Weaver & Taam (1980), and most recently by Woosley and Weaver (1994, hereafter WW94). This scenario was also suggested for the explanation of subluminescent Type Ia (WW94). Note that the explosion of a low mass WD was also suggested by Ruiz-Lapuente et al. (1993) to explain subluminescent SNe Ia but the mechanism for triggering of the central carbon detonation was not considered. Because low-mass WDs are much more common than massive WDs, the possible impact on our understanding of supernovae statistics and, consequently, the chemical evolution of galaxies must be noted. Moreover, based on light curve calculations with constant line opacities, Woosley and Weaver (1994) suspected that Helium detonations are commonly dimmer by about  $0.4^m$  with the obvious consequences for  $H_0$ .

To clarify the possible scenarios, the theoretical models must be tested by observations. Light curves and spectra of different scenarios for normal bright SNe Ia including detonations, delayed detonations, pulsating delayed detonations, and envelope models have been investigated in previous papers and compared with the observations (HKM91ab, KMH92; HMK93; KMH93; Müller & Höflich 1994; Höflich, Khokhlov & Wheeler 1995, Höflich 1995; hereafter HKM91, KMH92, HMK93, KMH93, MH94, HKW95 and H95 where H, K, M and W stand for Höflich, Khokhlov, Müller and Wheeler, respectively). We have investigated the validity and influence of the physical assumptions made in light curve and spectral calculations. The importance of a consistent treatment of the explosion mechanism, light curves and spectra became evident. We found that these normal bright supernovae show a small spread in  $M_V$ . These papers argued that different models are needed to explain the observations and  $H_0$  was derived to be  $66 \pm 10 km/secMpc$ . However, none of the previous models produced subluminescent SNe Ia as required to account for SN1991bg (see above). In a recent paper (HKW95), we have shown that the existence of a range of luminosities of Type Ia can be understood in the frame-

work of pulsating delayed detonation scenario. On the other hand, Woosley and Weaver suggested the class Helium detonations to be responsible for Type Ia Supernovae (see above). Moreover, detailed NLTE analysis of SN1994D showed that classical delayed detonation models may provide better fits to both the light curves and spectra, if the C/O white dwarf had a somewhat smaller central density than anticipated in our previous analyses (H95). So, in conclusion, the picture became somewhat confusing.

New, well-defined data even of very distant SN Ia have been published during the last two years. This allows for a much more comprehensive study than previously undertaken (MH94). New questions can also be investigated such as the suggestion by Bartlett et al. (1995) that  $H_0$  may show variations on large scales with a global value as low as 30 km/sec Mpc.

To address the problems raised above, one-dimensional models have been considered which encompass all currently discussed explosion scenarios. In section 2, our set of models is discussed, in particular, the Helium detonations. In section 3, general properties of the light curves are studied. In the following section, the influence of the red shift on the observations is discussed. In section 5, the method of comparison of models and observations and the individual comparisons are presented. Sections 6 and 7 focus on the relation between the type of the explosion and of the host galaxy and on the cosmological constants  $H_0$  and  $q_0$ . Finally, the results are summarized, the relation between type of explosion and the host galaxy is discussed and conclusions are drawn.

## 2. Models

A set of 37 SNe Ia parameterized explosion models has been considered which encompasses all currently discussed explosion scenarios (Table 1). The explosions are calculated using one-dimensional Lagrangian hydro with artificial viscosity (Khokhlov, 1991ab) and radiation-hydro codes including nuclear networks (Höfllich et al. 1995b). The latter code is based on our light curve code that solves the hydrodynamical equations explicitly by the piecewise parabolic method (Collela and Woodward 1984) and includes the solution of the radiation transport implicitly via the moment equations, expansion opacities similar to Karp, Lasher & Salpeter (1977), and a detailed equation of state. Radiation transport has been included to provide a smoother transition from the hydrodynamical explosion to the phase of free expansion. We omit  $\gamma$ -ray transport during the hydrodynamical phase because the high optical depth of the inner layers and the negligible energy input due to radioactive decay of  $^{56}\text{Ni}$  (Müller & Höfllich 1991, HMK92, HMK93, HKW95). Nuclear burning is taken into account using Thielemann's network (Thielemann, Arnould & Truran 1987, Cowan, Thielemann & Truran 1991 Thielemann, Nomoto & Hashimoto 1994 and references therein). During the hydro, a network of 20 isotopes is considered to properly describe the energy release. Based on a network of 216 isotopes, the final chemical structure is calculated by postprocessing the hydrodynamical model. The accuracy of the energy release has been found to be about 1 to 3 % in the reduced network compared to about 10 % for the approximations used previously (Khokhlov, 1991ab). For SNe Ia, the new code has been compared to previous results for several models, such as deflagration (DF1), classical delayed detonations (M35/37), and pulsating delayed detonations (PDD5/6). We note that radiation transport effects remain unimportant and only affect small scales even in models (PDD5/6) which enter the phase of homologous expansion on time scales of 10 to 60 minutes.

Based on the explosion models, further hydrodynamical evolution, and bolometric and monochromatic light curves are calculated using a scheme recently developed and widely applied to SN Ia (e.g. HKM91, KMH93, MH94). In principle, it is the same code as that described above, but nuclear burning is neglected and  $\gamma$  ray transport is included via a Monte Carlo scheme. The monochromatic colors  $B$ ,  $V$ ,  $R$ , and  $I$  are calculated using 100 discrete wavelength bands. For several models, detailed NLTE-spectra have been constructed (H95). The colors based on the NLTE atmospheres and LC calculations have been compared. Typically, the absolute errors in  $V$ ,  $B$ ,  $R$ , and  $I$  are below 0.05 to  $0.1^m$  near maximum light and remain between 0.2 to  $0.4^m$  at late time. Another uncertainty which affects the comparison with observations is due to the filter functions. For observations, any filter can be recalibrated to a set of standard stars, but the frequency response must be known to translate theoretical monochromatic fluxes into colors. In the

literature (Lamla 1982, Bessell 1990, Challis 1994), the transmission functions show wide variations, especially, for the infrared colors. For example, the I color may or may not cut off the region of the strong Ca II-IR emission. This has little influence on measurements of standard stars, but it will vastly change the color in SNe Ia, in particular, the strength of the secondary IR maximum. For more details see MH94 and HKW94. Previously, we used transmission functions as reconstructed at Vilnia (Lamla 1982). However, most of the modern measurements are based on Cousin’s functions as defined by Bessell (1990) which are used in this study. Small differences in  $M_V$  and related quantities with respect to previous studies can be understood by the change of the filter calibrations.

### 2.1. Explosions of massive white dwarfs

The first group of models consists of thermonuclear explosions of carbon oxygen white dwarfs close to the Chandrasekhar limit. We cover all scenarios being suggested including detonations (DET1/2, hereafter D-series), deflagrations (W7, DF1, DF1mix), delayed detonations (N21/32, M35-39; N- and M-series) and pulsating delayed detonations (PDD1-9; P-series). The deflagration speed is parameterized as  $D_{def} = \alpha a_s$ , where  $a_s$  is the local sound velocity ahead of the flame and  $\alpha$  is a free parameter. The speed of the detonation wave is given by the sound-speed behind the front. For delayed detonation models, the transition to a detonation is given by another free parameter  $\rho_{tr}$ . When the density ahead of the deflagration front reaches  $\rho_{tr}$ , the transition to a detonation is forced by increasing  $\alpha$  to 0.5 over 5 time steps bringing the speed well above the Chapman-Jouguet threshold for steady deflagration. For pulsating delayed detonation models, the initial phase of burning fails to release sufficient energy to disrupt the white dwarf. During the subsequent contraction phase, compression of the mixed layer of products of burning and C/O formed at the dead deflagration front would give rise to a detonation via compression and spontaneous ignition (Khokhlov 1991b). In this scenario,  $\rho_{tr}$  represents the density at which the detonation is initiated after the burning front dies out. Besides the description of the burning front, the central density of the WD at the time of the explosion is another free parameter. For white dwarfs close to the Chandrasekhar limit, it depends sensitively on the chemistry and the accretion rate  $\dot{M}$  at the time of the explosion. In a recent study on SN1994D (H95), evidence was found that the models with a somewhat smaller central density provide better agreement with both the observed spectra and light curves. Therefore, we have extended our grid of PDD models starting with lower central densities.

### 2.2. Merging white dwarfs

A second group of models is the outcome of the merger scenario (Webbink 1984; Iben & Tutukov 1984; Paczynski 1985). After the initial merging process, one low density white dwarf is surrounded by an extended envelope (Hachisu, Eriguchi & Nomoto 1986ab, Benz, Thielemann & Hills 1989). This scenario is mimicked by our



Table 1: Overview of investigated theoretical SNe Ia models. The quantities given in columns 3 to 11 are:  $M_\star$  white dwarf mass;  $\rho_c$  central density of the white dwarf;  $\alpha$  ratio of deflagration velocity and local sound speed;  $\rho_{tr}$  transition density at which the deflagration is assumed to turn into a detonation;  $E_{kin}$  final kinetic energy;  $M_{Ni}$  mass of synthesized  $^{56}Ni$ . In Model DF1MIX the composition was completely homogenized after burning had stopped. For the helium detonations, the mass is of the C/O core, and He-layers of the hydrostatic WD are given separately.

Model	Mode of explosion	$M_\star$ [ $M_\odot$ ]	$\rho_c$ [ $10^9 g cm^{-3}$ ]	$\alpha$	$\rho_{tr}$ [ $10^7 g cm^{-3}$ ]	$E_{kin}$ [ $10^{51} erg$ ]	$M_{Ni}$ [ $M_\odot$ ]	Symbol
DET1	detonation	1.4	3.5	—	—	1.75	0.92	*
DF1	deflagration	1.4	3.5	0.30	—	1.10	0.50	○
DF1MIX	deflagration	1.4	3.5	0.30	—	1.10	0.50	○
W7	deflagration	1.4	2.0	n.a.	—	1.30	0.59	○
N21	delayed det.	1.4	3.5	0.03	5.0	1.63	0.83	●
N32	delayed det.	1.4	3.5	0.03	2.6	1.52	0.56	●
M35	delayed det.	1.4	2.8	0.03	3.0	1.56	0.67	●
M36	delayed det.	1.4	2.8	0.03	2.4	1.52	0.60	●
M37	delayed det.	1.4	2.8	0.03	2.0	1.49	0.51	●
M38	delayed det.	1.4	2.8	0.03	1.7	1.44	0.43	●
M39	delayed det.	1.4	2.8	0.03	1.4	1.38	0.34	●
M312	delayed det.	1.4	2.8	0.03	1.0	1.35	0.20	●
PDD3	pul.del.det.	1.4	2.1	0.04	2.0	1.37	0.49	<i>bl.tr.</i>
PDD535	pul.del.det.	1.4	2.7	0.035	0.45	0.34	0.15	<i>bl.tr.</i>
PDD54	pul.del.det.	1.4	2.7	0.04	0.82	1.02	0.19	<i>bl.tr.</i>
PDD5	pul.del.det.	1.4	2.7	0.03	0.76	1.23	0.12	<i>bl.tr.</i>
PDD8	pul.del.det.	1.4	2.7	0.03	0.85	1.30	0.18	<i>bl.tr.</i>
PDD7	pul.del.det.	1.4	2.7	0.03	1.1	1.40	0.36	<i>bl.tr.</i>
PDD9	pul.del.det.	1.4	2.7	0.03	1.7	1.49	0.66	<i>bl.tr.</i>
PDD6	pul.del.det.	1.4	2.7	0.03	2.2	1.49	0.56	<i>bl.tr.</i>
PDD1a	pul.del.det.	1.4	2.4	0.03	2.3	1.65	0.61	<i>bl.tr.</i>
PDD1c	pul.del.det.	1.4	2.4	0.03	0.71	0.47	0.10	<i>bl.tr.</i>
HeD2	He-det.	0.6+0.22	.013	—	—	0.94	0.43	*
HeD4	He-det.	1.0+0.18	.150	—	—	1.50	1.07	*
HeD6	He-det.	0.6+0.172	.0091	—	—	0.72	0.252	*
HeD7	He-det.	0.6+0.14	.0089	—	—	—	—	goes "nova"
HeD8	He-det.	0.8+0.16	.025	—	—	1.08	0.526	*
HeD10	He-det.	0.8+0.22	.036	—	—	1.24	0.75	*
HeD11	He-det.	0.9+0.16	.061	—	—	1.37	0.87	*
HeD12	He-det.	0.9+0.22	.083	—	—	1.45	0.92	*
CO095	detonation	0.95	.016	—	—	1.10	0.18	*
CO10	detonation	1.0	.020	—	—	1.22	0.32	*
CO11	detonation	1.1	.04	—	—	1.44	0.58	*
DET2	detonation	1.2	0.04	—	—	1.52	0.63	△
DET2ENV2	det.+envelope	1.2 + 0.2	0.04	—	—	1.52	0.63	△
DET2ENV4	det.+envelope	1.2 + 0.4	0.04	—	—	1.52	0.63	△
DET2ENV6	det.+envelope	1.2 + 0.6	0.04	—	—	1.52	0.63	△

envelope models DET2ENV2...6 in which we consider the detonation in a low mass white dwarf surrounded by a compact envelope between 0.2 and 0.6  $M_\odot$ . For more details on these models see HKM92 and KMH93.

### 2.3. Explosions of sub-Chandrasekhar mass white dwarfs

We have included explosions of sub-Chandrasekhar mass white dwarfs (hereafter HeD-series), previously considered by several other authors (e.g. Nomoto 1980, 1982, Woosley, Weaver & Taam 1980, WW94, Livne 1990, Livne & Glasner 1990). Until now, no monochromatic LCs have been constructed for this class of models. Only WW94 calculated bolometric light curves, but under several restrictions, namely, omission of a detailed  $\gamma$ -ray transport, and, more importantly, the assumption that the line opacities are independent of the structure and time evolution of the expanding envelope. Note, that the influence of the opacities on the resulting LCs is comparable to the changes caused by different hydrodynamical models (HMK93).

For ease of comparison, we have used parameters close to those suggested by Woosley and Weaver (1994). To prevent repetition, we refer to the latter work for a detailed discussion of this class of models. Here, the basic assumptions and some technical details are outlined. About 278 depth points are used for the CO core. For the ignition of the carbon detonation, a good mapping is critical. To provide a resolution of roughly  $2 \cdot 10^{-5} M_{\odot}$ , the discretization in mass was increased logarithmically. This allowed for a higher resolution in the center by a factor of 10 compared to the outer layers. The initial chemical composition was 70%  $^{16}\text{O}$ , 29%  $^{12}\text{C}$ , 1%  $^{22}\text{Ne}$  by mass, and solar mass fractions of all other elements. We began with C/O white dwarfs of 0.6, 0.8, 0.9, and  $1.0 M_{\odot}$  with temperatures according to WW94 for the lower masses and Schaller et al. (1992) for the high mass. The accretion of Helium is calculated by our radiation-hydro code, where we neglect partial time derivatives to evolve a hydrostatic structure. The accretion rates are tuned such that about 0.16 and  $0.22 M_{\odot}$  of Helium are accreted when the thermonuclear runaway occurs at the bottom of the outer He layer. In general, our models resembled those of WW94 but we want to note that the final outcome depends very sensitively on details such as the exact amount of Helium. For the lowest mass white dwarf, the thermonuclear runaway occurred already at a time when only  $0.15 M_{\odot}$  had been accreted; whereas about  $0.17 M_{\odot}$  of He is required to trigger the central carbon detonation (Table 1). The discrepancy with WW94 may be explained by different discretizations, the numerical schemes, energy transport during the accretion phase of the white dwarf, or by nuclear rates, because the actual time of the explosion depends sensitively on the  $^{14}\text{N}(e^{-}, \nu)^{14}\text{C}$  rate. Within the uncertainties, we cannot rule out that, in reality, a larger amount of He can be accreted during the stellar evolution. Therefore, for this mass, we suppressed the runaway accordingly. The final velocity and density profiles and the chemical profile for the most abundant elements for several of our models are given in Figs. 1 and 2. Helium detonations show a qualitatively different structure in comparison to all models with a Chandrasekhar mass white dwarf. The intermediate mass elements are sandwiched by Ni and He/Ni rich layers at the inner and outer regions, respectively. Generally, the density smoothly decreases with mass because partial burning produces almost the same amount of kinetic energy as the total burning,

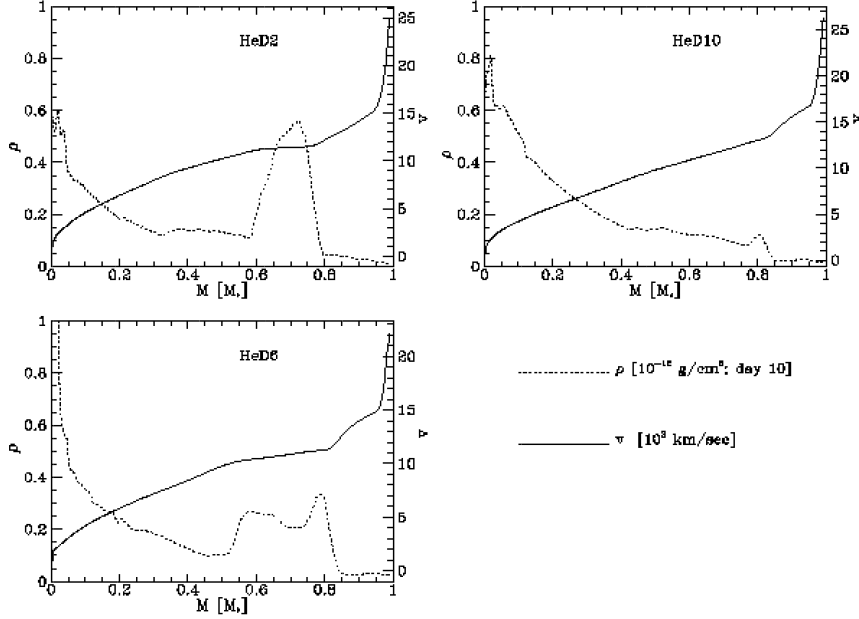


Figure 1: Density and velocity as a function of mass for the models HeD2, HeD6, and HeD10.

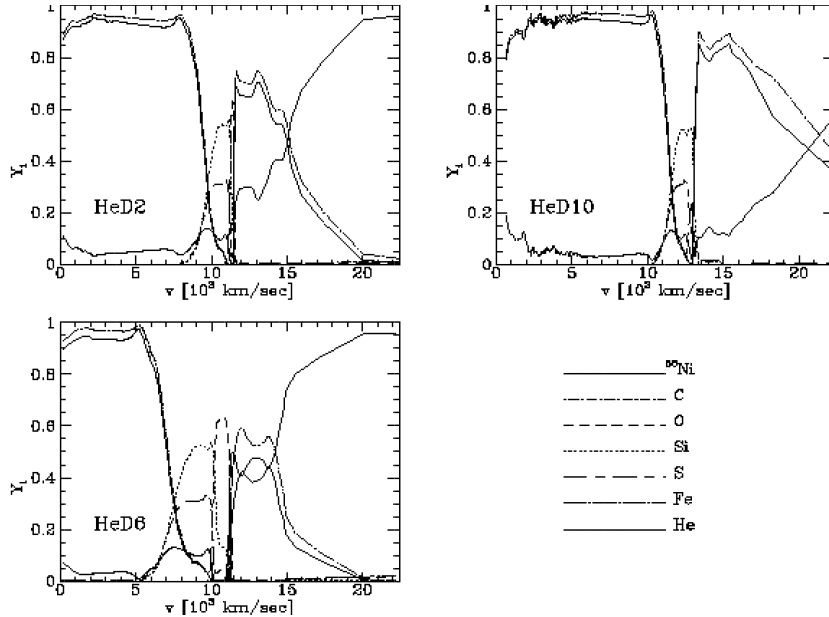


Figure 2: Final composition as a function of velocity for the models HeD2, HeD6, and HeD10.

but a moderate shell-like structure is formed just below the former Helium layers. Observationally, a distinguishing feature of this scenario is the presence of Helium and Ni with expansion velocities above  $11,000$  to  $14,000 \text{ km s}^{-1}$ . Typically, about  $0.07$  to  $0.13$  of Ni are produced in the outer layers, mainly depending on the mass of the Helium shell. Note the existence of a lower limit for the amount of Ni in the outer layers because of the requirements on the energy release to trigger the central carbon detonation. With increasing Helium mass, the subsequent central

compression and the size of the central region increase where, starting from an C/O rich mixture, the density becomes sufficiently high to burn carbon and oxygen up to  $^{56}\text{Ni}$ . For the same reason, i.e. the higher densities, the Ni production rises with increasing mass. Already the model HeD10 (Table 1) produces predominantly  $^{56}\text{Ni}$  and only little intermediate mass elements at velocities  $\leq 10000\text{km/sec}$  (Fig. 2). Therefore, models with a CO-core of more than  $0.9M_{\odot}$  can be ruled out from the observations.

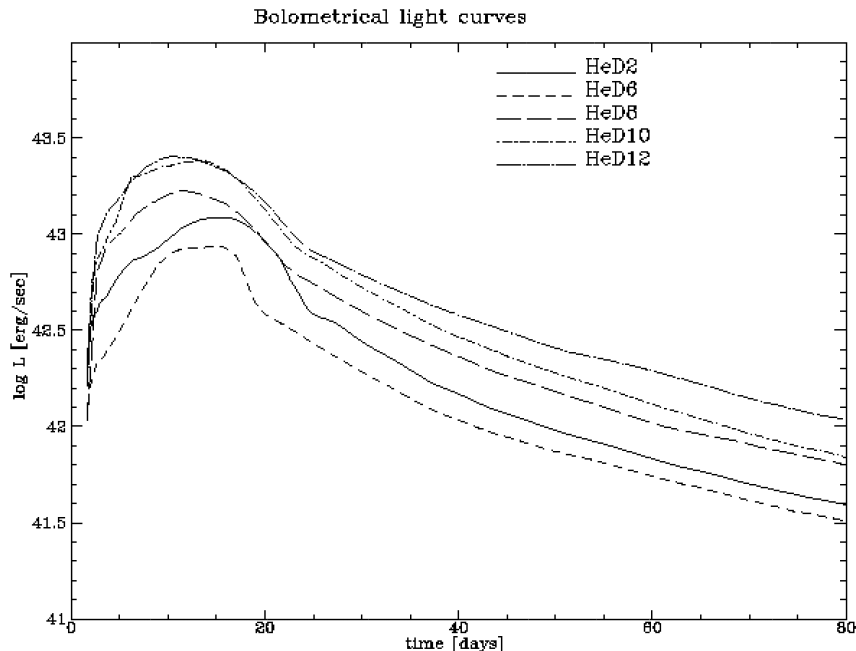


Figure 3: Bolometric light curves of some of the Helium detonation models (see Table 1).

Bolometric and monochromatic light curves are shown in Figs. 3 and 4. Helium detonations are capable of producing both bright and subluminous models. The characteristic of the light curves can be mainly explained by the presence of  $^{56}\text{Ni}$  at expansion velocities comparable to the photospheric velocities at about maximum light. Initially, the brightness increases rapidly. Often, a small plateau is formed because the contribution of the radioactive heating from the deeper layers is delayed due to the diffusion time scales. The first plateau is most pronounced in models with little outer helium, because those produce more intermediate mass elements. For the same reason, the final incline to maximum light is rather slow. Both for bright and subluminous models,  $^{56}\text{Ni}$  heating results in high color temperatures at maximum light (see table 2 and section 3). In general, the postmaximum decline is steep both in the bolometric and optical LCs due to the fast increase of the escape probability for gamma-ray photons and due to the rapid decay rate of  $^{56}\text{Ni}$  compared to  $^{56}\text{Co}$ . Note that the radioactive decay of the outer  $^{56}\text{Ni}$  contributes to the heating of the envelope well after the corresponding layers have passed the photosphere because the  $\gamma$  opacities are significantly lower than the optical opacity ( $1/35\text{cm}^2/\text{g}$  vs  $0.1\text{cm}^2/\text{g}$ ). Consequently, layers well beyond the optical photosphere receive

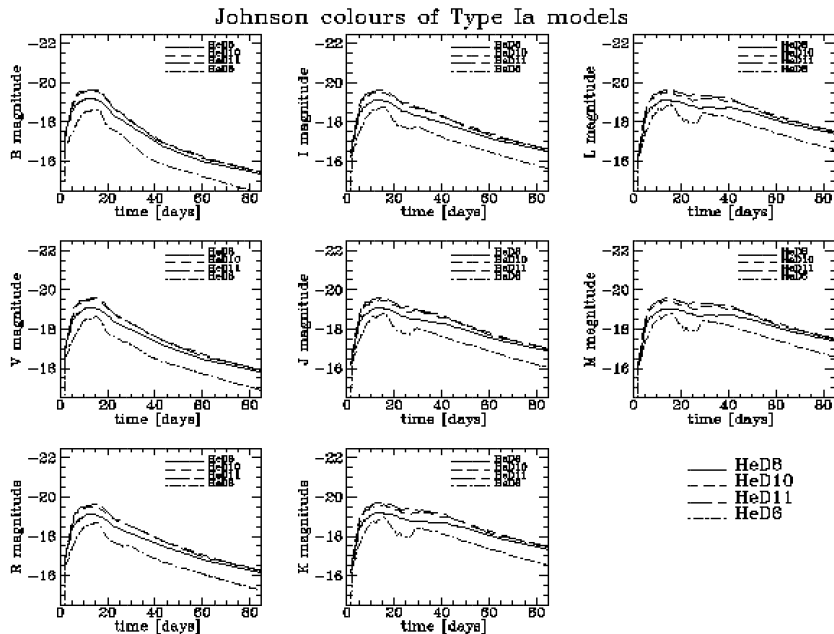


Figure 4: Monochromatic light curves in Johnson's color system.

energy. This additional energy source keeps the temperature and, consequently, the opacity at the photosphere sufficiently high to allow  $R_{ph}$  to increase well after maximum light. Consequently (Höflich et al. 1995), the monochromatic IR-light curves show secondary maxima even for subluminal models.

Note that a significant amount of the line emission at late phases should be powered by  $^{56}\text{Co}$  at high velocities. Even very subluminal SNe Ia must produce about  $0.1M_{\odot}$  of  $^{56}\text{Ni}$  in the outer layers. Thus, in the subluminal models, about 1/2 to 1/4 of the radioactive material is ejected at high velocities. This should show up in late-time spectra. In the layers where He and  $^{56}\text{Co}$  coexist, we suspect that Helium is partially ionized by secondary, high energy electrons from the  $\beta^+$ -decay of  $^{56}\text{Co}$ . Consequently, late time spectra may have a superposed Helium recombination spectrum. Whether Helium can recombine by charge exchange or collisions needs further investigations.

Table 2: Some observable characteristics of the models of Table 1. The quantities given in columns 2 to 9 are: The maximum bolometric luminosity  $L_{bol}$  in ergs/s, the rise time to bolometric maximum  $t_{bol}$  in days, the bolometric luminosity relatively to the energy generation by radioactive decay at  $t_{bol}$ , the absolute visual magnitude  $M_V$ , the rise time to visual maximum  $t_V$  in days, the color index B-V at maximum light, and the post-maximum decline rates  $dM_{15}$ ,  $dM_{60}$ , and  $dM_{100}$  in V over 15, 60, and 100 days.  $\Delta M_V(15)$  provides an estimate of the possible error (see text).

Model	$\lg L_{bol}$	$t_{bol}$	Q	$M_V$	$t_V$	B-V	$dM_{15} \pm \Delta dM_{15}$	$dM_{60}$	$dM_{100}$
DET1	43.51	7.5	0.76	-19.99	8.5	-0.06	.071 -.008+.011	.072	.045
DF1	43.18	13.5	1.03	-19.33	15.5	0.14	.080 -.003+.013	.062	.040
DF1MIX	43.17	7.3	0.62	-19.10	13.2	0.11	.059 -.033+.015	.057	.039
W7	43.30	14.0	1.20	-19.63	15.5	0.11	.079 -.016+.011	.069	.041
N21	43.41	10.7	0.87	-19.81	12.7	0.07	.052 -.008+.008	.052	.042
N32	43.27	14.5	1.21	-19.54	15.2	0.12	.083 -.007+.012	.068	.041
M35	43.30	13.5	1.03	-19.51	14.8	0.03	.053 -.015+.013	.056	.041
M36	43.31	13.3	1.15	-19.39	15.2	0.06	.059 -.009+.004	.060	.041
M37	43.24	13.5	1.17	-19.26	15.1	0.10	.064 -.007+.004	.058	.040
M38	43.15	13.8	1.15	-19.13	15.3	0.12	.067 -.011+.004	.059	.040
M39	43.06	14.3	1.22	-19.01	15.4	0.15	.073 -.013+.008	.059	.039
M312	42.75	12.0	0.87	-18.36	13.0	0.23	.052 -.007+.012	.054	.038
PDD3	43.28	15.0	1.46	-19.42	15.9	0.12	.054 -.003+.005	.051	.040
PDD535	42.51	17.8	0.97	-17.77	21.3	0.60	.046 -.010+.008	.038	.025
PDD54	42.71	12.3	0.84	-18.27	15.8	0.36	.058 -.008+.008	.057	.039
PDD5	42.54	11.2	0.84	-17.99	13.0	0.44	.087 -.010+.005	.067	.043
PDD8	42.71	11.5	0.85	-18.29	13.0	0.35	.064 -.012+.017	.066	.042
PDD7	43.01	11.3	0.83	-18.93	13.5	0.22	.056 -.013+.018	.065	.042
PDD9	43.27	10.3	0.76	-19.47	14.3	0.05	.056 -.018+.008	.058	.042
PDD6	43.21	12.7	0.94	-19.43	13.8	0.11	.054 -.012+.012	.059	.042
PDD1a	43.19	12.8	0.86	-19.38	14.1	0.09	.053 -.011+.005	.057	.042
PDD1b	42.73	11.8	0.87	-18.35	14.2	0.33	.073 -.012+.005	.067	.042
PDD1c	42.41	11.6	0.71	-17.73	13.8	0.53	.093 -.017+.005	.068	.044
HeD2	43.01	13.9	0.85	-18.99	15.9	+0.06	.108 -.008+.008	.075	.047
HeD6	42.91	14.4	1.17	-18.56	14.7	+0.05	.101 -.010+.004	.063	.047
HeD8	43.22	13.4	1.08	-19.21	13.8	-0.02	.071 -.009+.009	.058	.042
HeD10	43.38	13.2	1.07	-19.59	13.9	-0.01	.073 -.007+.007	.066	.044
HeD11	43.38	13.7	0.97	-19.62	14.1	-0.01	.075 -.008+.012	.067	.045
HeD12	43.40	11.5	0.80	-19.61	12.6	-0.04	.059 -.005+.005	.052	.039
CO095	42.82	11.7	1.11	-18.60	14.2	0.37	.092 -.012+.014	.074	.045
CO10	43.12	11.8	1.26	-19.00	14.0	0.25	.071 -.011+.005	.069	.044
CO11	43.24	11.9	0.93	-19.47	13.8	0.14	.061 -.008+.007	.065	.042
DET2	43.32	13.7	1.16	-19.67	14.2	0.14	.088 -.014+.011	.076	.045
DET2ENV2	43.27	16.6	1.24	-19.41	19.5	0.16	.049 -.011+.005	.042	.041
DET2ENV4	43.25	19.0	1.34	-19.31	21.1	0.20	.044 -.007+.009	.041	.040
DET2ENV6	43.21	19.3	1.26	-19.21	21.8	0.23	.042 -.006+.010	.040	.039

### 3. Comparison of theoretical light curves and observable relations

Although our light curve calculations are most reliable for the bolometric fluxes, this investigation will deal with monochromatic LCs.  $L_{bol}$  is uncertain from the

observations for epochs earlier than  $\approx 5$  days after maximum light, because a significant amount of the flux is emitted shortwards of the visual wavelength range (Branch & Tammann 1992). Different scenarios have been studied in previous works, and the new ones, including the Helium detonations, can be understood in full analogy. Therefore, we restrict our discussion to some particular points and the display of some useful relations based on the entire sample.

Models can be discriminated by their monochromatic light curves (Fig. 5 and 6), in particular, by the shape before day 60. As a general trend, the maxima of subluminal supernovae are more pronounced. The reason becomes obvious if we consider the following related point. In the literature (Arnett, Branch and Wheeler 1985), the so called Arnett’s law (1982) has been used to determine  $H_0$  under the assumption that SN Ia are standard candles. This law states that the bolometric luminosity  $L_{bol}$  is equal to the instantaneous release of energy by radioactive decay  $L_\gamma$ , i.e.  $Q = L_{bol}/\dot{E}_\gamma \approx 1$  independent of the underlying physical model. Consistent with our earlier works (KMH93), we find that  $Q$  depends on the model because the opacities vary strongly with temperature (HMK93). Typically,  $Q$  varies from 0.7 to 1.4 (Table 2 and Fig. 7). Note that, in previous works, the related quantity  $\tilde{Q}$  was defined as  $L_{bol}$  compared to the instantaneous energy deposition by radioactive decay.  $\tilde{Q}$  is larger by about 5 to 25 % compared to  $Q$  depending on the escape probability of  $\gamma$  rays. Whereas  $\tilde{Q}$  is a measure of the energy gain due to the opacity effect,  $Q$  contains both the effects of the opacity and the increasing escape probability for  $\gamma$  photons which distinguish Arnett’s analytical approach from our calculations. For models with fast rising LCs, the opacity stays high and the photosphere recedes mainly by the geometrical dilution of matter. For models with a slower rise time or little  $^{56}\text{Ni}$ , the opacity drops strongly at about maximum light. The photosphere recedes quickly in mass, and thermal energy can be released from a region, being larger than in the first case. Consequently, the maximum is more pronounced, and the  $\tilde{Q}$  exceeds unity. Because no additional energy is gained, the energy reservoir is exhausted faster, and the post-maximum decline becomes steeper.

Independent of details of the explosion mechanism, the current models have rise times between 11 to 14 and 13 to 16 days in  $L_{bol}$  and  $V$ , respectively. Longer rise times of up to 22 days require pulsating delayed detonations and envelope models which have a dense, shell-like structure. The low-mass WDs close to  $0.6 M_\odot$  can also produce some shell structure (Fig.1). Models with  $M_{Ni} \geq 0.4 M_\odot$  are similarly bright within a narrow strip of  $\approx 0.5^m$  (Fig. 8).  $M_V$  is rather insensitive to  $M_{Ni}$  and the spread in  $M_V$  at a given  $M_{Ni}$  is comparable to the change of  $M_V$  with  $M_{Ni}$ . If less  $^{56}\text{Ni}$  is produced,  $M_V$  strongly declines with  $M_{Ni}$  with a similar rate both for massive and low mass WDs. Although as a general tendency, the brightness seems to increase within each series of models, the variations are not monotonic even within a given type of explosion. E.g. the delayed detonation model N32 is brighter than M36 despite its lesser  $^{56}\text{Ni}$ . Below  $0.4 M_\odot$ , the overall spread in  $M_V$  remains about the same.

The subluminal models tend to be much redder at maximum light than normal bright SNe Ia. This is generally independent of the explosion mechanism (Fig. 8) because the radioactive heating by  $^{56}\text{Ni}$  is highly reduced. The exceptions are Helium detonations of low-mass WDs (see last section). Note that  $^{56}\text{Ni}$  heating occurs independently from details of the explosion, because a Helium detonation will produce predominantly  $^{56}\text{Ni}$  even if multidimensional effects become important (Livne 1990). This provides a clear distinction between explosions of sub- and Chandrasekhar mass white dwarfs. The effect on the late time spectra was discussed in the previous section. For possible consequences for CO formation, see HKW 95.

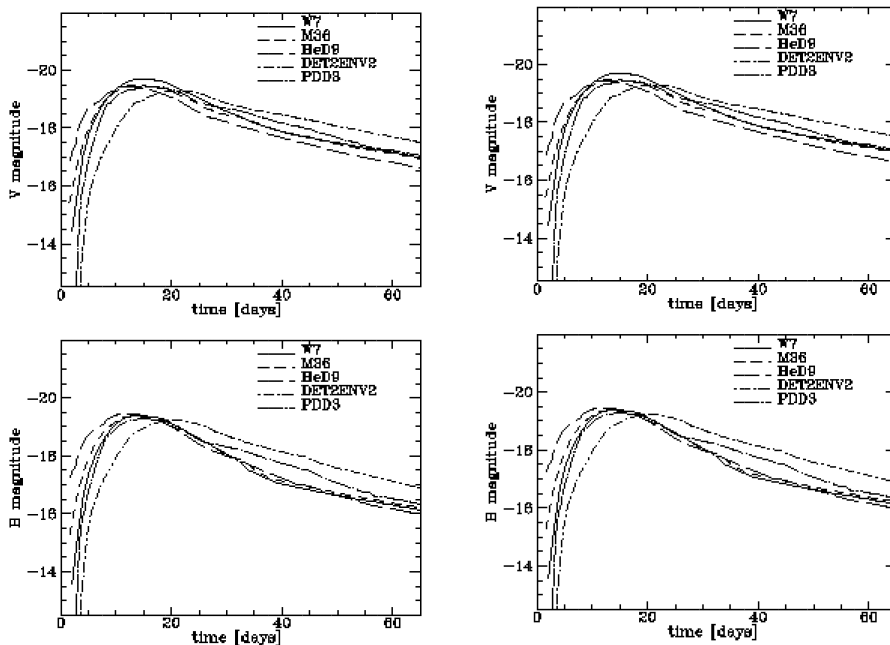


Figure 5: Monochromatic B and V light curves of normal bright supernovae of deflagration (W7), classical delayed detonation (M36), Helium detonation (HeD9), envelope (DET2ENV2), and pulsating delayed detonation (PDD3) models.

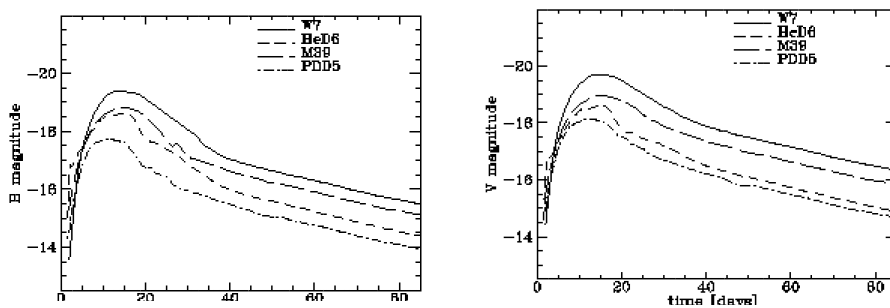


Figure 6: Monochromatic B and V light curves of subluminal supernovae for pulsating delayed detonation (PDD5), classical delayed detonation (M39), and Helium detonation (HeD6) models. For comparison, the deflagration model W7 is given.



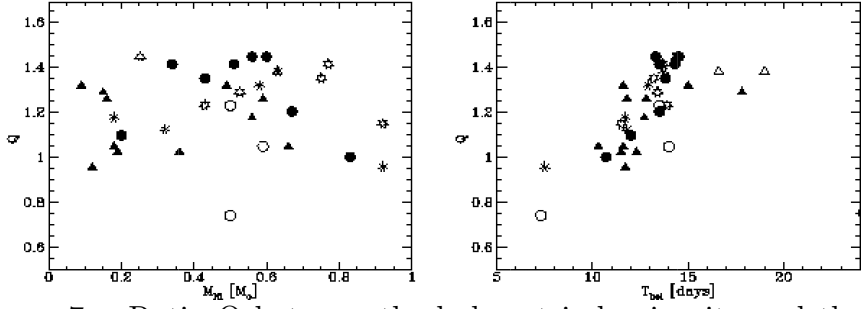


Figure 7: Ratio  $Q$  between the bolometric luminosity and the energy release by gamma decay at  $t_{bol}$  as a function of the  $^{56}\text{Ni}$  mass (left) and rise time to bolometric maximum  $t_{bol}$ . The different symbols correspond to different explosion scenarios (see Table 1).

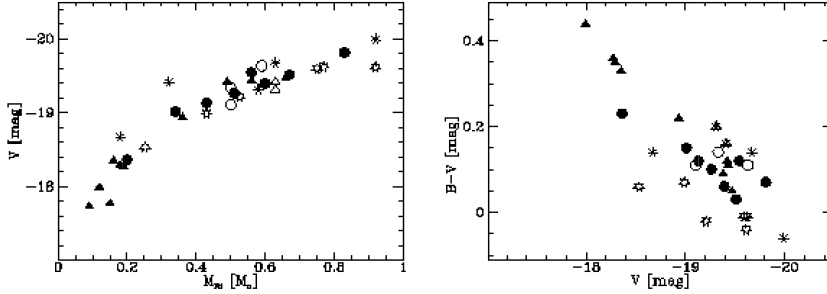


Figure 8: Absolute visual brightness  $V$  as a function of the  $^{56}\text{Ni}$  mass (left) and intrinsic color  $B-V$  as a function of  $V$  (right).

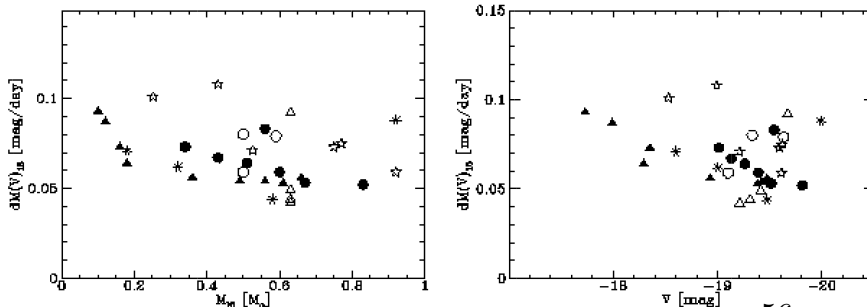


Figure 9: Decline rate  $dM_{15}(V)$  as a function of the  $^{56}\text{Ni}$  mass (left) and as a function of  $V$  at maximum light.

The relations between the post-maximum declines  $\Delta m_{15}(V)$ ,  $\Delta M_{60}(V)$ , and  $\Delta M_{100}(V)$  and the Ni mass and absolute brightness  $M_V$  are shown in Figs. 9 and 10. We use the decline in  $V$  instead of  $B$  as suggested by Phillips (1993) because  $B$  depends sensitively on the filter functions and the metallicity of the progenitor. Because several of the light curves have flat maxima,  $\Delta M_V(15)$  is sensitive to errors in the time of maximum light. The latter may be affected by differences in the filter functions, cosmological red shifts, and the uncertainties inherent to our light curve calculations. To estimate the size of errors, we allowed for a shift in time

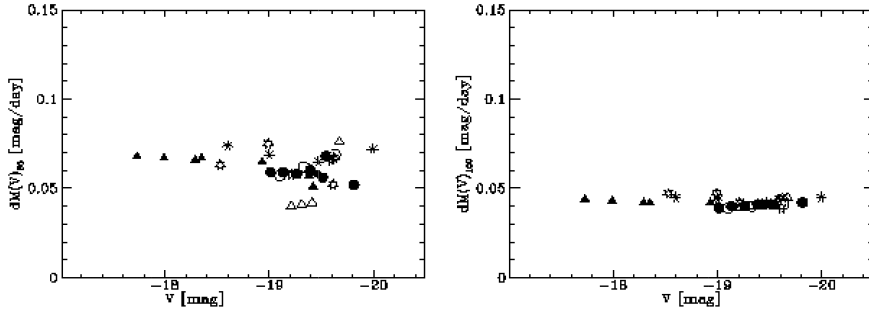


Figure 10: Decline rate  $dM_{60}(V)$  and  $dM_{100}(V)$  as functions of  $V$  at maximum light.

corresponding to a change of  $0.05^m$  in  $M_V$ . The early decline is mainly governed by the receding photosphere. Within each series of models,  $dM_V(15)$  becomes larger with decreasing  $^{56}\text{Ni}$  mass and, thus, with increasing  $M_V$ . In total, a spread of roughly  $0.5^m$  must be expected for the  $M_V(dM_V(15))$  relation. For  $\Delta M_{60}$ , the time base always reaches the linear tail produced by the  $^{56}\text{Co}$  decay, but the relative contribution of the linear tail varies. This breaks the overall monotonicity in the trends. Finally,  $\Delta m_{100}$  is insensitive to both the underlying model and the absolute brightness because it is governed by the radioactive decay of  $^{56}\text{Co}$ .

#### 4. Cosmological redshift

Before the comparison with observations, we want to address the question of the influence of the cosmological red shift both on the shape of light curves and on the correction factors for the interstellar reddening.

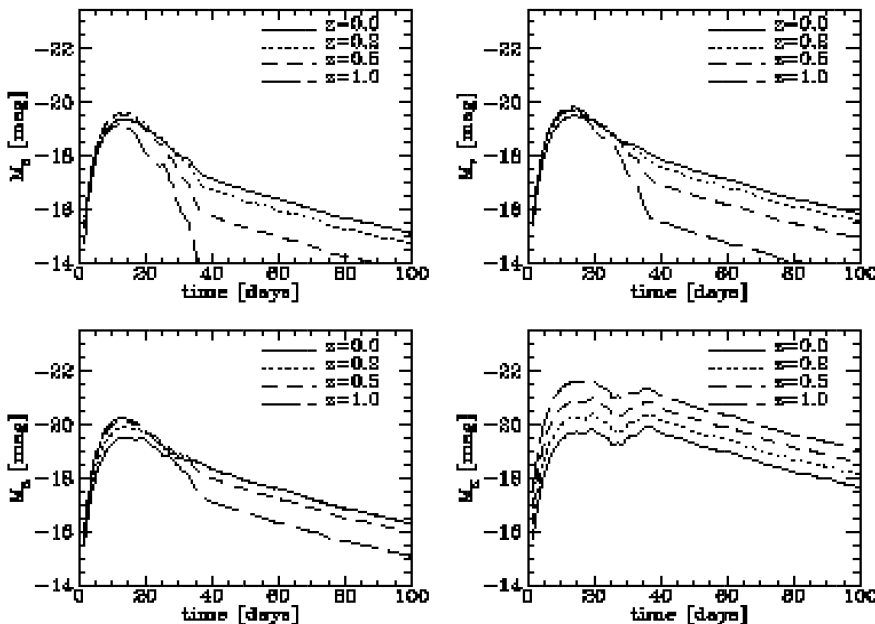


Figure 11: Monochromatic optical and infrared light curves of the delayed detonation model M36 at different cosmological red shifts.

The cosmological expansion has two main effects – the frequency shift and the stretching of the spectrum. The former causes a change in the shape of the light curves because the overall energy distribution of supernovae varies strongly during the first month – namely, line blocking at shorter wavelengths increases with time. Therefore, post-maximum declines in B and V become steeper with increasing  $z$  (Fig. 11). Note that the frequency shift does not imply that observed magnitudes can be translated directly from one color to another, because magnitudes do not provide an absolute measure for the fluxes, but brightnesses normalized to an A0V star. The stretching of the spectra causes an overall dimming of the flux over a given filter range. Note that our corrections (Figs. 12 & 13) are consistent with the empirical k-corrections of Hamuy et al (1993a).

From the models, the overall flux distribution is given. Therefore, k-corrections are consistent with the information from the light curve and spectra. In principle, we must not expect uncertainties related to the k-correction to grow with distance, as it is inherent for all purely statistical methods where the k-correction must be estimated from local supernovae. This may be regarded as an advantage for using models because the k-corrections show large individual variations of the order of 0.3

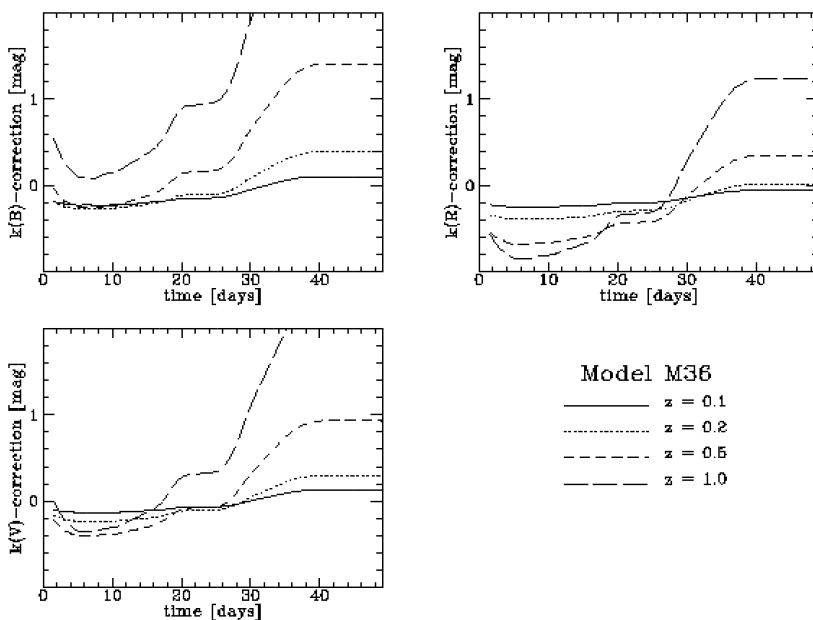


Figure 12: k-correction for different red shifts  $z$  as a function of time for M36.

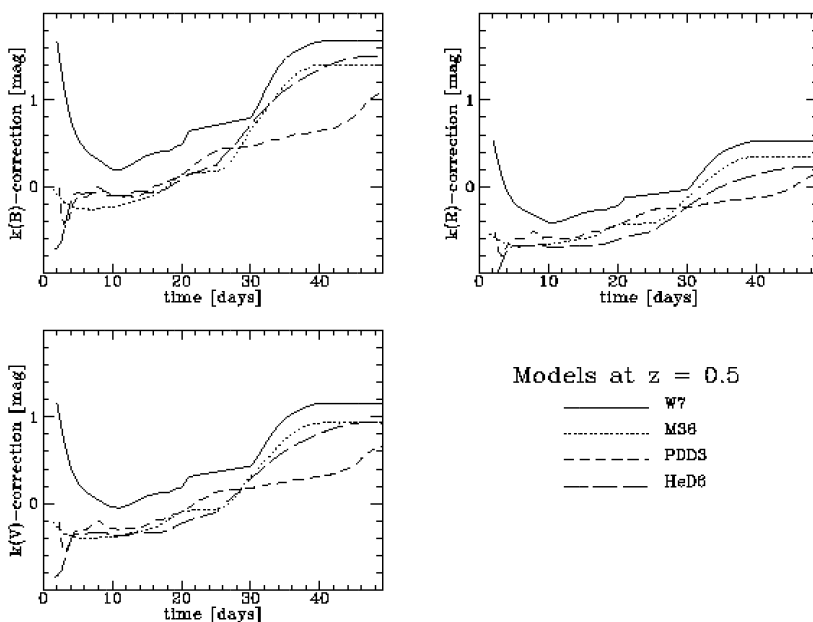


Figure 13: k-correction as a function of time for different models at  $z=0.5$ .

... 0.4 mag at about maximum light for  $z=0.5$  even for ‘normal’ bright supernovae (Fig. 13, see also Hamuy et al. 1993b). Note that, before day 5 to 10, the k-correction decreases for all models but the Helium detonations. Except for the latter models,  $^{56}\text{Ni}$  is concentrated towards the center and the radioactive heating of the photosphere is delayed. In Helium detonations,  $^{56}\text{Ni}$  in the outer layers keeps the temperature high from the very beginning.

For distant supernovae, the correction for interstellar reddening depends on the

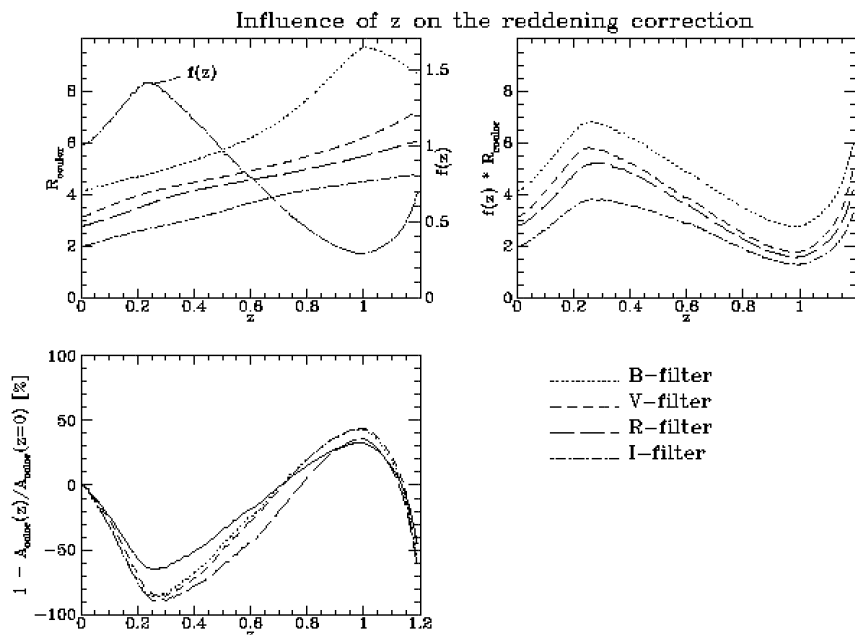


Figure 14: Influence of the cosmological red shift  $z$  on the value for the extinction coefficient  $R_{color}$  (eq. 1) and the correction factor  $f(z)$  (upper left) and the combined effect on the relation between color excess and extinction (upper right). In addition, the error is given if the  $z$ -correction is neglected (lower graph).

spatial distribution of the absorbing interstellar material. In light of the determination of  $q_0$  and the high accuracy needed, it may be useful to look at the possible influence of  $z$ . The cosmological expansion has two main effects: a) a photon, emitted at a redshift  $z$ , sees the absorption law at a redshift  $z'$  of the absorbing material, and b) the differential absorption between colors changes. Thus, the extinction  $A_{color}$  due to the interstellar medium at a redshift  $z'$  is given by

$$A_{color} = R_{color,z'} f_c(z) E_{B-V} \quad (1)$$

where  $R_{color,z'=0}$  is the ratio between  $E_{B-V}$  and the extinction. The factor  $R_{color,z'}$  takes into account the cosmological redshift  $z'$  of the absorbing material (Fig. 14) and  $E_{B-V}$  is the measured color excess. The function  $f_c(z)$  corrects for the differential change with  $z'$  between the B and V.

In the general case of  $n$  clouds at redshifts  $z'_1 \dots z'_n$ , eq. 1 becomes

$$A_{color} = \sum_{i=1}^n R_{color,z'_i} f_c(z'_i) E_{B-V,i} \quad (2)$$

where  $E_{B-V,i}$  gives the relative contribution of a particular cloud. In principle,  $E_{B-V}$  must be determined independently, e.g. by the relation between the line absorption from UV-lines and their redshifts. In practice, the likely cases are that the absorption happens within our galaxy ( $z' = 0$ ) and within the parent galaxy ( $z' = z$ ) (or a linear superposition of both). The contribution from our own galaxy

can be measured independently. Obviously (Fig. 14), the influence of  $z$  on the reddening correction must be taken into account because the resulting, systematic error is comparable to the size of the reddening correction itself. For example, an  $E_{B-V} = 0.05^m$ , if determined for a supernovae at  $z=0.2 \dots 0.4$ , would translate into an error of  $0.15^m$  in  $M_V$ . Note the possible errors for  $q_0$ .

## 5. Comparison of theoretical and observed light curves

It is necessary to confront our parameterized models with observations because not all scenarios may be realized in nature. The main aim is to get some insight into the physics of the explosion and progenitor evolution. Individual comparisons help to answer questions about the flame propagation and the progenitors of SN Ia, i.e. whether they have masses close to the Chandrasekhar limit, originate from low-mass objects, or may be understood in the framework of the merging scenario. It may be interesting to ask for the spread among all models that are found to resemble observations.

In the following comparison we have considered the full set of SNe Ia explosion models (see Table 1). The following supernovae are analyzed: SN 1937C, SN 1970J, SN 1971G, SN 1972E, SN 1972J, SN 1973N, SN 1974G, SN 1975N, SN 1981B, SN 1983G, SN 1984A, SN 1986G, SN 1988U, SN 1989B, SN 1990N, SN 1990T, SN 1990Y, SN 1990af, SN 1991M, SN 1991T, SN 1991bg, SN 1992G, SN 1992K, SN 1992bc, SN 1992bo, and SN 1994D. This sample consists of almost all SNe Ia for which very good light curves have been published or which are interesting for distance determinations. The observational data were mainly selected from the compilations of Ciatti & Rosino (1978), Barbon et al. (1989a), and Cadonau & Leibundgut (1990), Filippenko et al. (1992ab), and from the CTIO supernovae search (Phillips et al. 1987, Hamuy et al. 1993a, 1994, Wells et al. 1994). We refer to these compilations for a detailed discussion of the individual measurements and for references to the individual observers. If additional data are used, we will refer to the original literature. Note that this sample includes six SNe Ia measured at Asiago in the 1970s (SN 1970J, SN 1971G, SN 1972J, SN 1973N, SN 1974G, SN 1975N). Due to problems with the absolute calibration of the B color, the apparent brightness  $m_B$  may be underestimated by up to several tenths of a magnitude (Turratto 1995, private communication). In principle, an increase of the brightness in B leads to an overestimate of distances. However, at the same time, the interstellar reddening is systematically underestimated, which has the opposite effect. Therefore, we assume symmetric, large error bars for the SNe Ia observed at Asiago (Müller & Höflich 1994).

The criterion determining the “best” theoretical model for a given observed supernova is the best overall agreement between the shape of the calculated and the observed monochromatic light curves. Thus, the “best” theoretical model is not determined by the distance-dependent absolute maximum magnitude of the supernova, but by light curve characteristics, for example, the pre-maximum behavior, the width of the maximum, the rate of the steep post-maximum decline, and the rate of the subsequent linear decline.

Before we quantify these criteria, we have to address the question of fitting an individual model to a given set of observations and to determine the following

parameters: a) the time of the explosion  $t_o$ , b) the distance  $d$ , and c) the interstellar reddening  $E_{B-V}$ . In general, we base our fitting procedure on the B and V colors because they are very sensitive to the interstellar reddening, a consistent set of data is available, and filter functions are probably closest to the standard system.

A horizontal shift of the theoretical light curves provides information on the moment of the explosion. A vertical shift of provides information on the monochromatic distance module, i.e.

$$m_{color} - M_{color} = 5 \log \frac{d}{10pc} - 5 + A_{color} \quad (3)$$

where  $d$  is the distance,  $A_{color}$  is the interstellar extinction, and  $color$  stands for B, V, R, or I. The interstellar reddening law ( $R_{color} = A_{color}/E_{B-V}$ ) for our Galaxy gives  $R_B = 4.0$  where its frequency dependence can be taken from Savage & Mathis (1979). The general applicability of these values is debated. From a statistical analysis of SNe Ia, Jöeveer (1982) derives  $R_B = 1.8$ . Capaccioli et al. (1990) derive a similar value but with a large uncertainty ( $R_B = 1.7 \pm 1.4$ ). Della Valle & Panagia (1992) conclude from a detailed discussion of the previous studies and from their own study of SNe Ia that  $R_B = 3.35 \pm 0.75$  ( $2\sigma$ ), which is consistent with the value derived for our Galaxy. However, all supernovae-based estimates rely on the invalid assumption of SNe Ia being standard candles. The differences with respect to the Galactic values are likely produced by this incorrect assumption. Therefore, we use the Galactic value and extinction laws for all wavelengths from the UV to the IR range. If our estimate of  $E_{B-V}$  is smaller than the uncertainties inherent in our models (see above), we neglect the intrinsic reddening within the host galaxy and use the value for the Galactic extinction towards the parent galaxy  $\tilde{E}_{B-V}$  given by Burstein & Heiles (1984).

In previous comparisons, we have fitted theoretical and observed light curves by visual inspection (HKM91, KMH92, MH94, HMKW1995b) to find the best overall agreement. This could be justified because the non-homogeneity of the light curve data overshadowed the benefits of a sophisticated fitting procedure. In this paper, a more quantitative approach is used because several well observed LCs became available. In principle, the most straightforward way would be the ‘classical’ procedure where each observational point has the same statistical weight and the standard deviation  $\chi$  is minimized, i.e.

$$\tilde{\chi} = \sqrt{\frac{\sum_{j=B,V} \sum_{i=1}^{n(j)} \chi_{i,j}^2}{(n_B + n_V)(n_B + n_V - 1)}} \quad (4)$$

with

$$\chi_{i,j} = |M_{model,color} - M_{obs,color}| \quad (5)$$

where  $M_{model,color} - M_{obs,color}$  is the distance modulus at the time  $i$  for a given distance  $d$  and interstellar reddening and  $n_B$  and  $n_V$  are the number of observations in V and B, respectively.



The direct approach becomes questionable if the coverage of the LCs is incomplete, if the data-points are unevenly distributed and if errors both in models and measurements are neglected. To overcome the former problems, we minimize the time average of the time integrals of the standard deviation, i.e.

$$\tilde{\chi} \rightarrow \bar{\chi} = \sum_{j=B,V} \int_{t=t1_j, t2_j} F(\chi(t)) dt \quad (6)$$

where  $t1_j$  and  $t2_j$  are the dates of the first and last observation of color  $j$ . To reconstruct  $F(\chi(t))$ , we rectify the irregularly sampled data set  $[t_j, \chi_j]$  by means of Wiener filtering based on a fast algorithm (Rybicki and Press 1995). This allows for a consistent solution within the Newton-Raphson iteration for  $t_o$ ,  $E_{B-V}$  and  $d$ . Wiener filtering requires the definition of a correlation length  $w_i$ . The  $w_i$  of the LC varies strongly with time. Consequently, any reconstruction would be effected by the assumed correlation length. However, the correlation length is expected to vary only slightly if we consider the change of the standard deviation. The correlation length  $w_i$  of  $\chi_i$  can be assumed to be constant. The remaining errors are small because the resulting function  $F(\chi)$  depends only in second order on  $w_i$ . Our ansatz is equivalent to the assumption that  $w_i$ , for the reconstruction of the observed LCs, is given by the theoretical LCs. Obviously, for successful models, this approach is valid. For unsuccessful models, our procedure may give wrong fitting parameters (i.e.  $t_o$ ,  $M - m$  and  $E_{B-V}$ ) but those models are excluded due to their large  $\bar{\chi}$  (see below).

Following the discussion on the accuracy of the monochromatic colors based on the models, the error  $\bar{\varepsilon}_{color}$  is assumed to be  $0.05^m$  and  $0.1^m$  for V and B, respectively. After maximum light, a corresponding linear increase in the error is taken to be  $0.0025$  and  $0.007 mag/day$ , respectively. The error  $\varepsilon_{obs,color}$  is estimated from the scatter in the observations and the accuracy given by the specific observation.

For each model,  $t_o$ ,  $d$  and  $E_{B-V}$  are iteratively determined by a Newton-Raphson scheme to minimize  $\bar{\chi}$ . Two more restrictions are introduced. In several cases, the supernova was discovered on photographic plates or in the R color. Then, in the fitting procedure, the time of the explosion is forced to be prior to the first detection. If the galactic contribution to the reddening were known, this value provides a lower bound for  $E_{B-V}$ . The infrared light curves are used for consistency checks.

Now, we want to address the question of defining acceptable models or, more appropriately, of the defining criteria to reject certain models. As mentioned earlier, the shape of the early LCs is very model dependent. We demand the following criteria: a) post-maximum declines  $dM_{15}(V)$  and  $dM_{60}(V)$  are consistent (see Table 2); b) If pre-maximum LCs are observed, the slope up to maximum must be consistent; c) The maximum of  $\chi_{i,B/V}$  is within  $3\sigma$  error bars; d) The infrared colors are consistent with the observations within the error bars, e)  $\bar{\chi}$  is smaller than  $\bar{\chi}_{obs,B,V}$ ; and e) photospheric expansion velocities, as inferred from spectra,

agree with the models.

The dependence of the photospheric radius and of the photospheric expansion velocity  $v_{ph}$  as a function of time can also be used to test explosion models and, in particular, it can be used to separate “non-standard” from “standard” models (HMK93, KMH93, H95). In some cases (SN1988U, SN1994D), detailed NLTE-spectra are constructed and compared with observations. A detailed spectral analysis of 27 SNe Ia for different dates is beyond the scope of this paper. Detailed studies of spectral peculiarities even of elements such as Ti are needed to get good spectral fits. In turn, this would call for good spectral time coverage (H95) which is rarely available. To include the information of the photospheric velocity, we have used a somewhat more simple approach for the majority of supernovae. The velocity  $v_{ph}$  can be measured directly by the Doppler shift of spectral lines. A comparison based on the velocities thus determined should only be regarded as a guideline, for the following reasons. Line photons are emitted at larger radii than continuum photons. Consequently, different lines form in different layers above the photosphere. Secondly, the line forming region is not only determined by temperature and density, but also by the radial profile of the abundances. For example, the change of  $v_{ph}$  implied by the Si II line is less than that inferred from the Mg II line (see, e.g., SN 1989B in Fig. 16). This effect is more pronounced during later epochs when the ejecta become transparent. Thus, most weight should be given to the early epochs near maximum light when the line forming region is compact. In addition, the expansion velocities are based on measurements of the Doppler shift corresponding to the minimum flux of a certain feature but the result may be influenced by NLTE-effects (Höflich, 1990). Finally, in our models, the photospheric velocity is taken at a Rosseland optical depth of 2/3; however, at some frequencies, the line forming region is located at smaller radii. From our detailed NLTE-analysis of SN1994D, the total error must be expected to be of the order of 10 to 15 %.

Often, more than one theoretical model reproduces the observations within the uncertainties (see Table 3). Sometimes because the overall structures are rather similar (N32/W7) or, sometimes, they are based on the same explosion mechanism. For instance, in case of SN1972E, both delayed detonation models M35 and N21 allow for a quantitatively similar fit. Following Table 1, this must be interpreted as follows: this specific supernova can be understood within the delayed detonation scenario from a C/O white dwarf close to the Chandrasekhar limit and a central density of about  $2.8...3.5 \cdot 10^9 \text{ g cm}^{-3}$ , and the transition from the deflagration to the detonation happens at the high densities of about  $3...5 \cdot 10^7 \text{ g cm}^{-3}$ .

### 5.1. Previously analyzed supernovae

In previous studies, the following set of supernovae have been analyzed and discussed in detail: SN 1937C, SN 1970J, SN 1971G, SN 1972E, SN 1972J, SN 1973N, SN 1974G, SN 1975N, SN 1981B, SN 1983G, SN 1984A, SN 1986G, SN 1989B, SN 1990N, SN 1991T, SN 1991bg, SN 1992bo, SN 1992bc, and SN 1994D (Höflich et al. 1992, Khokhlov et al. 1992, MH94, Höflich et al.1994, H95). The early

systematic studies of the first 13 objects were based on a subset of 11 models with  $^{56}\text{Ni}$  masses above  $0.52 M_{\odot}$ . As for the rest of this sample, subluminous SNe Ia have been considered, but the mechanism of Helium detonations was not. For SN 1991bo, SN 1991bc, and SN 1991bg, only pulsating delayed detonation models were considered in HKW95. Therefore, all SN Ia are re-analyzed with our full set of models, including Helium detonations using our new quantitative fitting procedure to overcome one of the main points of criticism of the earlier works.

In general, our previous results are confirmed - namely, the changes in the time of the explosion, distances, reddening corrections and models ranges remained well within the former error bars. Yet, as a tendency, delayed detonation models with a somewhat smaller central density (M-series) provide better fits than the old N-series. For several bright and slightly subluminous SNe Ia, Helium detonations of sub-Chandrasekhar mass white dwarfs between  $0.6$  and  $0.9M_{\odot}$  cannot be ruled out from the light curves but they can be excluded by early spectra or the minimum velocity of Si (e.g. SN1972E). In the corresponding model, the photosphere would be formed in or just below the Ni-rich layers. Test calculations based on our NLTE-code confirmed this result, i.e. the synthetic spectra did not come close to the observations.

In the following, we want to discuss three supernovae of the old sample in more detail because either our new models provided a better understanding of the object or the data sets have been improved.

In our earlier study of SN1991bg, we found agreement between the subluminous pulsating delayed detonation model PDD5 with  $0.12M_{\odot}$  of Ni. Harkness was able to reproduce the spectra at about maximum light by his LTE models (Wheeler et al. 1995). However, there was some quantitative disagreement in the B light curve, and the IR-emission at maximum light was systematically too dim by about  $0.15^m$  to  $0.2^m$  in I and R, respectively. We find a somewhat better agreement with the new model PDD1c which produces slightly less Ni ( $0.10M_{\odot}$ ). Still, a possible problem persists. We need a rather large reddening. Despite the fact that, for low photospheric temperatures, the intrinsic color is very sensitive to the temperature, we do not think that a further reduction of the overall energy distribution could solve the problem. Instead, we favor the following two ‘physical’ solutions. The extra extinction may be produced by dust-formation in subluminous SNe Ia. In principle, dust can form at early phases. Whether it can persist is under investigation (Dominik et al., 1995). Another possibility for very red colors at maximum light is selective line blanketing, mainly caused by Ti II lines (Branch, private communication). To answer these questions, detailed spectral analyses by NLTE models are under way.

As for the distance moduli, the differences with respect to our previous works are always well within the error range, i.e. less than  $0.1^m$ , with the exception of SN1972E. For this supernova, the very first observation in the B filter implied a very rapid rise and a slow decline, ruling out all models but the delayed detonation model N21 in which a large amount of Ni is produced which, therefore, is located close to the surface. Recently, Leibundgut (1993, private communication) re-analyzed this

observation and found the first measurement to be about  $0.5^m$  brighter. This, in turn, allows better fits by models with a slower rise. Although SN1972E is still at the bright end of SN Ia, this reduces the distance by about 10...15%.

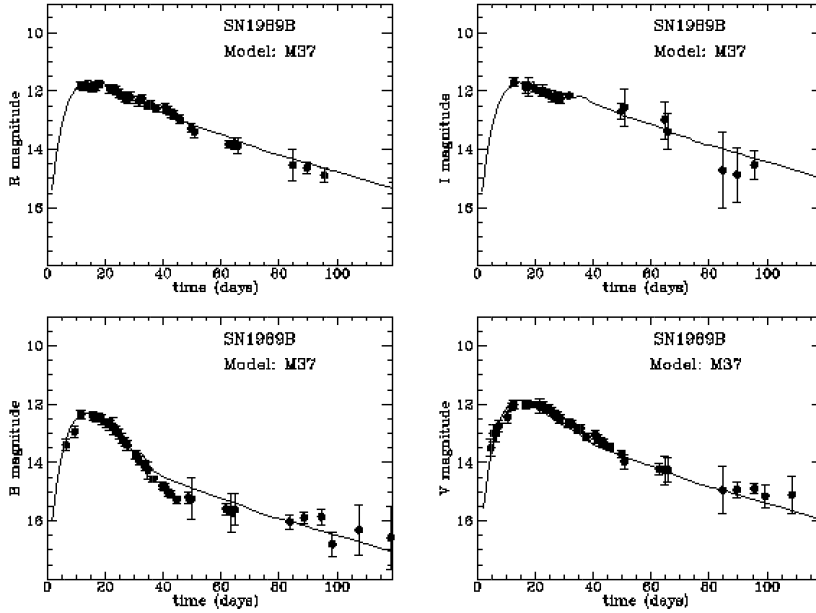


Figure 15: Monochromatic light curves of SN 1989B band compared with the calculated light curve of the delayed detonation model M37. The 2 sigma-error ranges are given by Wells et al. (1994)

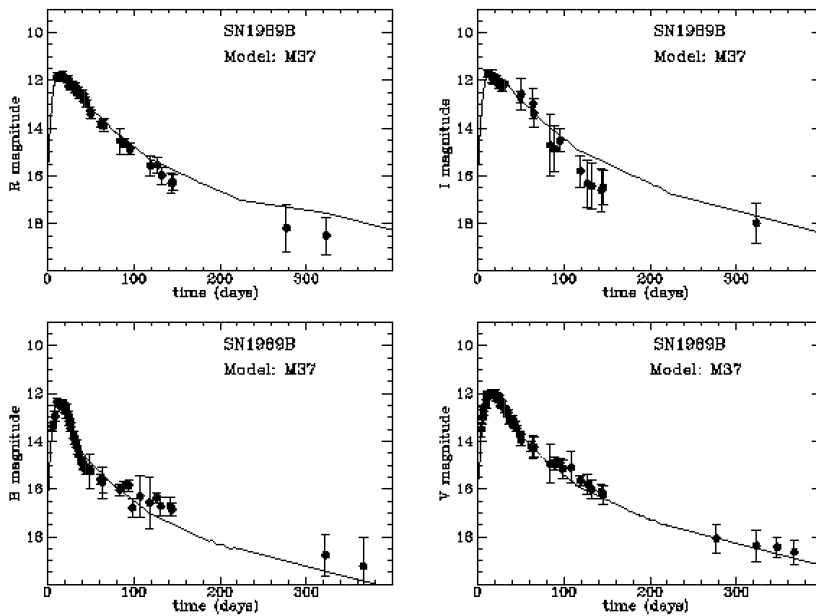


Figure 16: Same as 15 but including the late times.

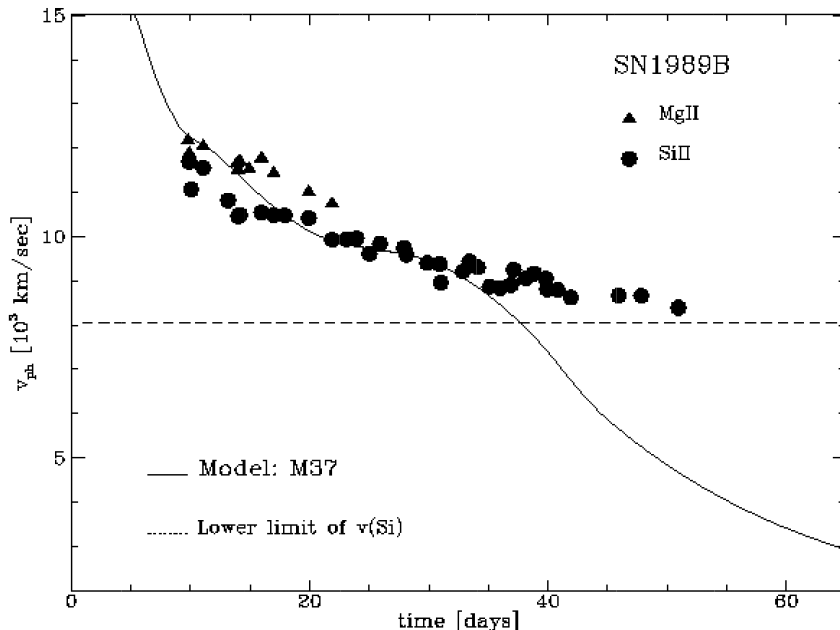


Figure 17: Photospheric velocity of the delayed detonation model M37 in comparison with the expansion velocities implied by the line shifts of Mg II and SiII. The dotted line is the velocity at which, in M37, the Si abundance has dropped to 10 % of its maximum value.

One of the earliest detections relatively to the time of maximum light of any Type I a supernova is SN1989B. The first observation ( $m_V \approx 17^m$ ) on SN 1989B in NGC 3627 is available from a pre-discovery image taken by Marvin & Perlmutter (1989) at JD 2447549.5. This epoch is about 15-16 days before  $V$  maximum ( $V_{max} = 12.0^m$ ) implying that the rise time to maximum is very well known. Unfortunately, measurements of  $V$  obtained by different authors show discrepancies of  $\approx 0.4^m$  (Barbon et al. 1990). Recently, a very homogeneous data set was published that provides an excellent coverage both of optical and infrared light curves and spectra (Wells et al. 1994). The photometry is mainly based on observations at CTIO with its well-defined set of filters. The light curves and photospheric expansion velocities can be reproduced by the delayed detonation model M37 and, somewhat less successful by M36 (Figs. 15-17). After about day 120, the decay of the light curves follows the radioactive decay of  $^{56}\text{Co}$ . Note that, at late times, the theoretical LCs are uncertain because of our approximate treatment of the energy distribution. The observational error bars increase strongly for later times. Thus, the good agreement with the late time light curves must not be given great weight. Early on, the photospheric velocity (Fig. 17) can be measured by the SiII and MgII lines at  $6355\text{\AA}$  and  $4481\text{\AA}$ , respectively. The velocities indicated by the MgII line and of the SiII line stop following the receding photosphere at day 25 and 35, respectively, because of the decrease of the Si and Mg abundances. The best agreement between calculated and observed monochromatic light curves can be obtained for SN 1981B if an interstellar reddening of  $E_{B-V} = 0.45^m$  is assumed. This value is significantly larger than the color excess resulting from the intergalactic extinction

towards the parent galaxy  $\tilde{E}_{B-V} = 0.01^m$  (Burstein & Heiles 1984). It must be attributed to the intrinsic extinction of the parent galaxy which is highly inclined. Our value is comparable to the estimates of Wells et al. (1994), but it is significantly smaller than the estimates of Barbon et al. (1990;  $0.70^m \dots 0.95^m$  with a mean value of  $0.81^m$ ) because their value is determined using a standard light curve. The distance to NGC 3627 resulting from our models is  $8.7 \pm 3$  Mpc.

### 5.2. SN 1988U

SN 1988U was discovered on August 9, 1986 at  $V \approx 22.05^m$  in a faint member of the distant cluster AC118 at a redshift of  $z=0.31$  (Norgaard-Nielsen et al. 1989). Subsequently, this object was monitored in V and R over a period of about 2 months down to about  $24.4^m$ . Based on the spectrum taken about 10 days after the discovery, this object was clearly identified as a Type Ia event (Norgaard-Nielsen et al. 1989). Up to now, it represents the most distant SN Ia for which good measurements including spectra have been published. Although the database does not exactly match our criterion of a well-observed SN Ia, we have included this object to demonstrate the advantage of a simultaneous analysis of light curves and spectra for the distance determination of faint SNe Ia.

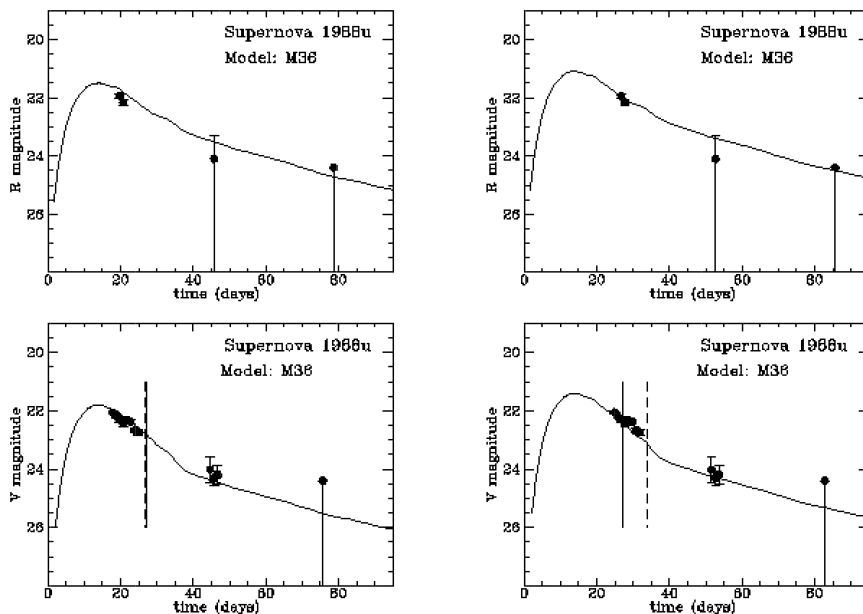


Figure 18: Monochromatic V and R light curves of SN 1988U in comparison with the calculated light curve of the delayed detonation model M36. The dashed line marks the time when the photospheric velocity of the models corresponds to the observed line shift (thin line). The right and left plots correspond to different time shifts. Both fits of the LC reproduce the observations, but the right fit can be ruled out by the spectrum.

We assumed a redshift of  $z=0.31$  and corrected our light curves accordingly.

From the post-maximum decline, and the observation at about day 40 after the explosion, all bright delayed detonation models (i.e. N21/M35) and ‘normal bright’ envelope and pulsating delayed detonation models can be ruled out. Very slowly declining models are in conflict with the upper limit for the brightness at late times. On the other hand, both subluminal and Helium detonation models decline too fast past maximum light to allow for an agreement between the measurements at about day 20 and 40. Additionally, for subluminal models, the photosphere has receded too far to be consistent with the observed line shifts of Si II at  $6355 \text{ \AA}$ . This leaves the classical deflagration model W7 and the delayed detonation models N32/M36 as good candidates (Fig. 18). An interstellar extinction  $E_{B-V}$  of  $0.055^m$  for AC118 (Knude 1977) is consistent with our upper limit of  $0.12^m$ . The advantage of a simultaneous analysis of light curves and spectra is evident: Judging from the light curves, both fits are equally good, but the time of the explosion is not well defined. This effect alone causes a 30% uncertainty in the distance. However, the right fit is inconsistent with the photospheric velocity. We get a distance of  $1.44 \pm 0.25 \text{ Gpc}$ .

### 5.3. SN 1990T

SN 1990T was discovered by Antezana in the galaxy PGC 63925 on July 21, 1990 shortly after maximum light. Accurate photometric measurements in B, V, R, and I are available spanning a period of about 4 months (Hamuy et al. 1995). Two spectra, 5 and 26 days after the discovery, are taken. At the first date, the line shift of the SiII feature at  $6355 \text{ \AA}$  indicates a photospheric expansion velocity of  $\approx 8700 \text{ km/sec}$ .

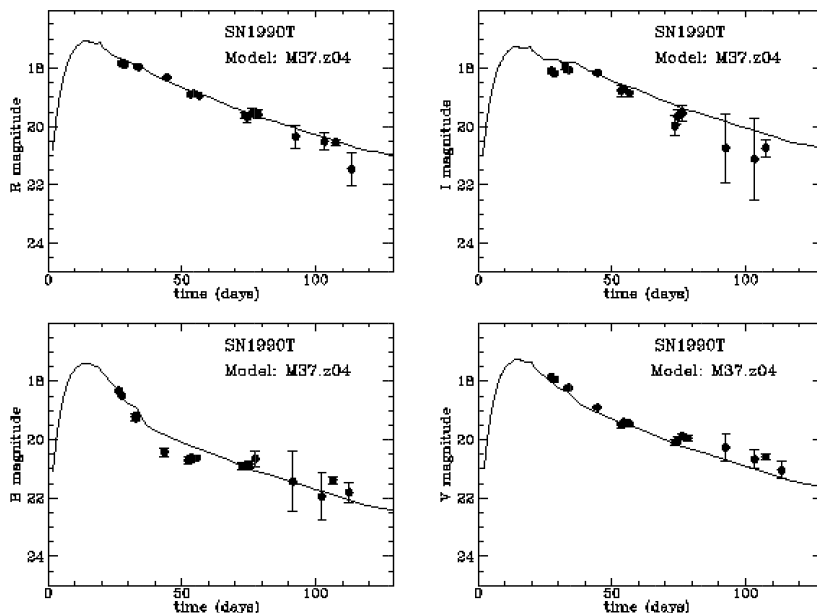


Figure 19: Monochromatic light curves of SN 1990T filter band compared with the calculated light curve of the delayed detonation model M37.

The optical and infrared light curves can be well reproduced by the delayed

detonation models with a Ni production between  $0.43$  to  $0.60 M_{\odot}$  (Fig. 19). From the fits, the time of the discovery can be determined to be about two weeks after maximum light. The expansion velocity is consistent with the previous estimate but hardly provides further restrictions on the models. However, our analysis favors models with Ni masses at the lower end for ‘normal’ bright supernovae. Due to the cosmological red shift, the B color of the models is rather uncertain because, for slightly subluminal models, the corresponding wavelength range is very sensitive to line blanketing. This explains some of the problems at about day 50. The V,R and I colors provide best fits for  $E_{B-V} = 0.0^m$  but B calls for  $E_{B-V} = 0.1^m$ . Based on the intrinsic brightness of models M38 to M36, the distance to PGC 5128 is  $180 \pm 30$  Mpc.

#### 5.4. SN 1990Y

SN 1990Y was found by Wischnjewski (Hamuy et al. 1995) in an anonymous elliptical galaxy on August 22, 1990 about two weeks after maximum light. BVRI photometry is available over the subsequent period of 3 months (Maza et al. 1994, Hamuy et al. 1995). One week after the discovery, spectra were taken (Della Valle et al. 1990). The Doppler shift of the Si II line at  $6355 \text{ \AA}$  corresponds to a photospheric expansion velocity of about  $9000 \text{ km/sec}$ .

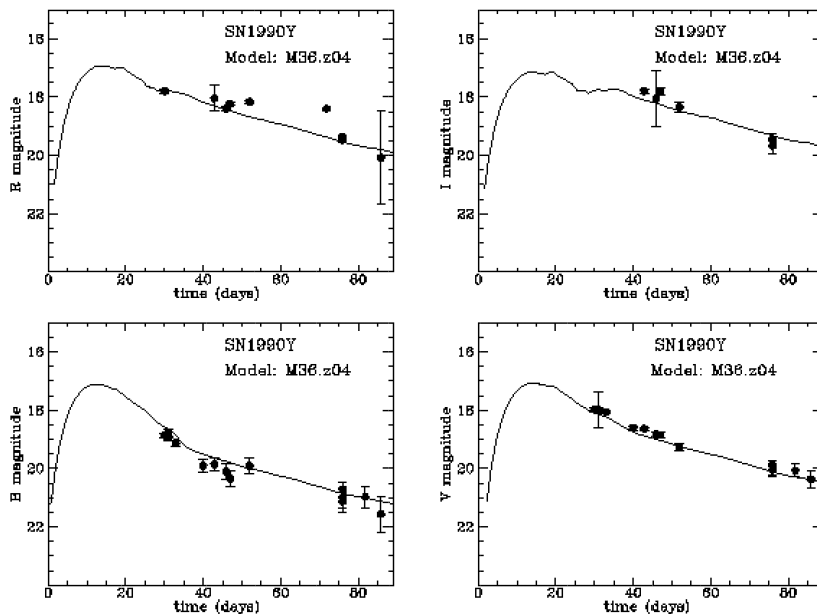


Figure 20: Monochromatic light curves of SN 1990Y compared with the calculated light curve of the pulsating delayed detonation model M36 at a redshift of 0.04.

Due to the lack of measurements, there is hardly any restriction on the type of the explosion, i.e. pulsating, delayed detonation, and deflagration models can reproduce the light curves (Fig.20). However, strongly subluminal models can be ruled out based on the infrared colors and the high expansion velocities of Si II seen two to three weeks past maximum light. The colors are compatible with little



interstellar reddening. Based on the intrinsic brightness of models, the distance is  $195 \pm 45$  Mpc.

### 5.5. SN1990af

We find that the B and V light curves can be reproduced within the error bars by the classical deflagration model W7 and the delayed detonation models N32/M36/M37 if we correct for the cosmological expansion and an interstellar reddening of  $E_{B-V}$  of  $0.05^m$  (Fig. 21). SN 1990af is well within the range of normal bright supernovae. Subluminous models can be ruled out because of their narrow maxima.

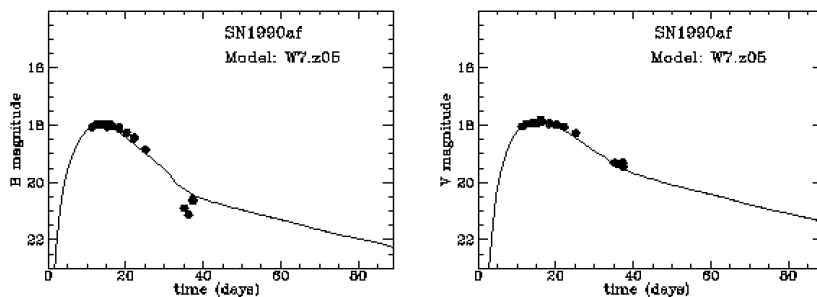


Figure 21: Monochromatic light curves of SN 1990af compared with the calculated light curve of the pulsating delayed detonation model W7.

SN 1990af was discovered in an anonymous elliptical galaxy at  $z=0.0503$  on October 24, 1990 well before maximum light. BV photometry is available over the following month. Spectra taken right after the discovery imply a photospheric expansion velocity of 12,040 km/sec (Hamuy et al. 1995).

In our models,  $z=0.05$  causes a sufficiently large change in the shape of the light curve whereas Hamuy et al. (1993b) found that their k-corrections based on calibrated templates are insufficient. Our agreement does not necessarily imply that our k-correction is more reliable due to uncertainties in our models for wavelengths shortwards the B band. The distance is determined to be  $265 \pm 85$  Mpc. The huge error range is attributed to the fact that only a few of our models can be ruled out and, consequently, the successful models cover the entire brightness strip for 'normal' SNe Ia.

### 5.6. SN 1991M

SN 1991M was discovered in the spiral galaxy IC1151 on March 12, 1991 by the Berkeley Automated Supernovae Search (Pennypacker et al. 1991). First colors were reported by Hook and McMahon (1991) about 3 days later. V, R, and I photometry were published by Ford et al.(1993), mainly obtained at the Leuschner, Whitin, and VanVleck observatories starting about 9 days after the discovery. Note that the very small error bars (Ford et al., 1993) seem to be somewhat optimistic. In many instances, measurements differ by several sigma even if taken at the same time.

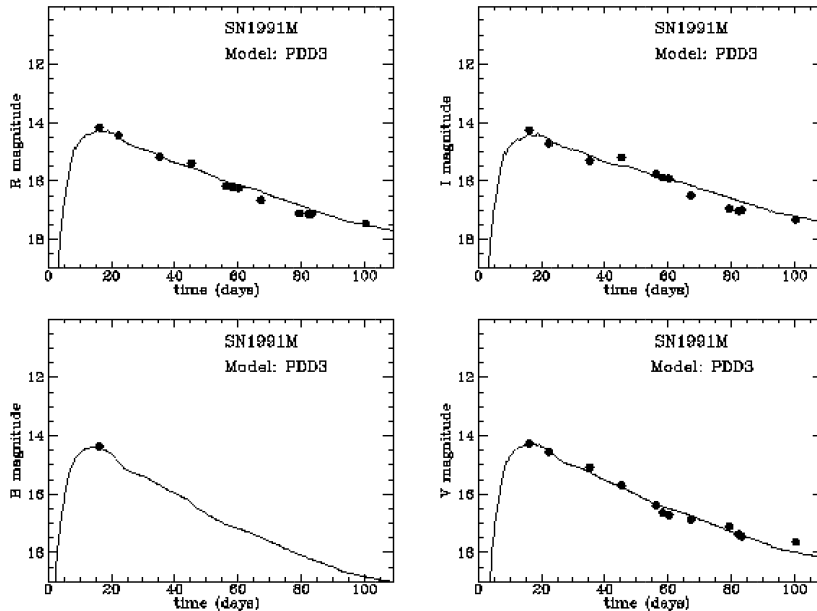


Figure 22: Monochromatic light curves of SN 1991M compared with the calculated light curve of the pulsating delayed detonation model PDD3.

In the infrared, this may be explained by different transmission functions. We assume an observational error of  $0.1^m$  and  $0.2^m$  for the V and the infrared colors, respectively. The rather slow post-maximum decline in V cannot be reproduced by delayed detonation models in which the transition to the detonation occurs at low densities, but requires M35. In principle, the bright delayed detonation model N21 reproduces the post-maximum decline, but its IR flux is too small. Similar small declines can also be produced by strongly pulsating delayed detonation models. The lack of measurements at and before maximum light and of spectra disallow distinguishing between the alternative models. In conclusion, both the optical and IR light curves can be reproduced by strongly pulsating model PDD3 (Fig. 22) or the bright delayed detonation model M35. The secondary IR maxima in I is too weak in the models. A possible explanation may be that the transmission function of I is somewhat broader compared to Bessell's (1990) calibration, and, consequently, the Ca II-IR triplet emission contributes to the observed flux in I (HKW95). According to our fits,  $E_{B-V} = 0.12^m$ . This value should be taken with caution because it is based on one B measurement. This uncertainty accounts for a large error in the distance of  $41 \pm 10$  Mpc.

### 5.7. SN 1992G

SN 1992G was discovered by Shunji Sasaki, Hasaki-machi, and Ibaraki on February 9, 1992 in the spiral galaxy NGC 3294 at a photographic magnitude of about  $14^m$  (Kosai 1992). A similar brightness was found on a photographic plate from February 7, 1992 by Sasaki (Kosai 1992) suggesting that SN1992G was close to maximum light at that time. Our analysis is based on the V, R, and I photometry

of Ford et al. (1993) which provides excellent coverage of the subsequent three months. The B and V colors at about 2 and 4 weeks after the discovery have been determined photographically by Tsvetkov (1994).

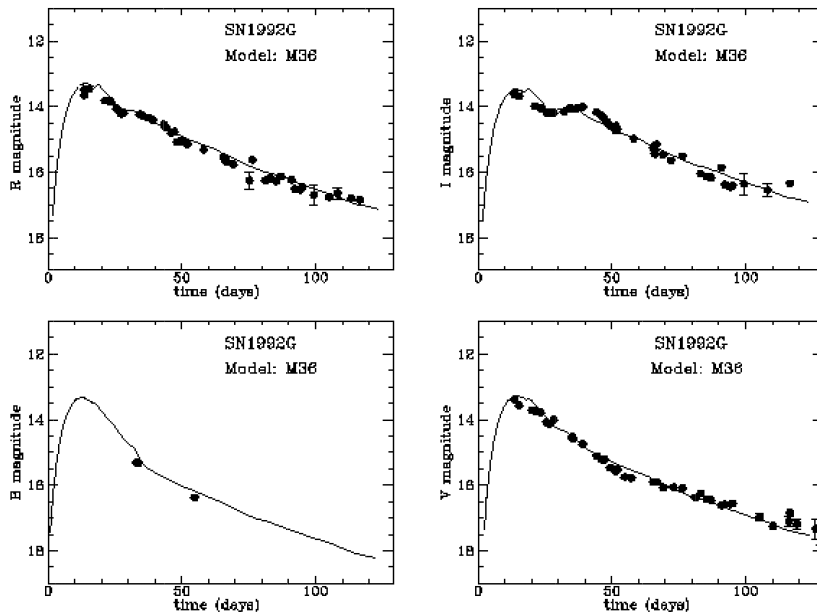


Figure 23: Monochromatic light curves of SN 1992G compared with the calculated light curve of the delayed detonation model M36.

On February 21, spectra by Iijima, Turatto and Cappellaro (1992) were taken. The SiII feature indicated an expansion velocity of about 10000 km/sec. The light curves and the expansion velocity can be well reproduced by our delayed detonation model M36, although the secondary maximum in I is too weak. The discrepancy may be explained by differences in the I filter (see last section). Besides the strong secondary IR-peak, the observations also can be fitted by the pulsating delayed detonation model and even Helium detonation models. Clearly, the different models could be distinguished from the early light curves because the models predict very different slopes (see Fig. 5-6). Our fits are consistent with a reddening  $E_{B-V} = 0.05^m$ , but this value is based on photographic B colors. The distance to NGC 3294 is  $21 \pm 6$  Mpc.

### 5.8. SN 1992K

SN 1992K was found on March 3, 1992 in the SBb galaxy ESO- 269-G57 on a photographic plate by Antaezana (Hamuy et al. 1994). Starting about three days after the discovery, this object was continuously monitored during the following 5 months both spectroscopically and in the BVI colors (Hamuy et al. 1994). Spectra taken right after the discovery indicate a photospheric expansion velocity of 9085 km/sec. Both the spectral peculiarities and the red continuum suggest that SN 1992K is almost a twin of the strongly subluminous supernova 1991bg (Filippenko et al. 1992ab, Leibgundgut et al. 1993).

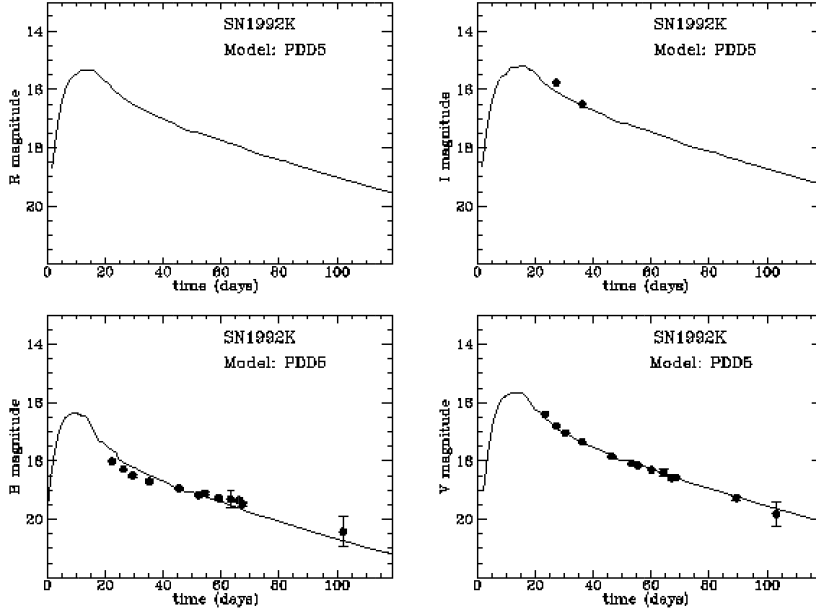


Figure 24: Monochromatic light curves of SN 1992K compared with the calculated light curve of the pulsating delayed detonation model PDD5.

We find that the B and V light curves can be reproduced within the error bars by the same strongly subluminal models as SN1991bg. However, PDD5 tends to provide a better fit than PDD1c. The intrinsic reddening is found to be  $0.18^m$ , i.e. larger than the Galactic reddening correction in the direction of the host galaxy ( $0.04^m$ , Burstein & Heiles 1982). Based on the intrinsic brightness of models, the distance is  $43_{-8}^{+15}$  Mpc. For subluminal SNe Ia, the brightness depends sensitively on the actual amount of  $^{56}\text{Ni}$ . This explains the rather large error bars for this well-observed object.

## 6. Explosion mechanism and type of the galaxy

It is interesting to relate the type of the host galaxy with the explosion scenario. Here, we distinguish ellipticals from spirals and irregular systems. Because, in general, ellipticals consist of stars with main sequence masses less than  $\approx 3M_{\odot}$  but, in the latter groups, massive stars are also present, this may provide important information on the progenitor evolution.

In total, about 18 spirals, 5 ellipticals and 2 irregular galaxies are in our sample (see Table 3). For the galaxy in AC 118, no classification is available. The classical deflagration model W7 and delayed detonation hereafter (hereafter group I) are simultaneously able to reproduce the light curves of several SNe Ia. The same is true for pulsating models and envelope models (group II). In spirals and irregular galaxies, both groups are represented, but group I is more frequent than II (12:7). For ellipticals, the relation is reversed (1-2:3). SN Ia of group II are highly favored. The possible two candidates (SN 1990Y and SN 1990af) of group I in ellipticals are in anonymous galaxies at about 200 to 270 Mpc making the classification of the type of the galaxy rather uncertain. We note that, for bright supernovae, the mean brightness of group II is systematically fainter by about 0.1 to 0.2<sup>m</sup>.

Although our sample is still too small to draw final conclusions, comparisons of this kind may be regarded as a promising way to get a link to the stellar evolution of the progenitors.

Table 3: List of observed Type Ia supernovae used in our sample. Columns 2 to 7 give the parent galaxy, its type, peculiar velocity  $v_z$  according to the MERCG catalogue (Kogoshvili 1986), the distance modulus of the host galaxy and the color excess  $E_{B-V}$  of the SNe Ia as determined from our models. In column 8, we give names of those theoretical models (see Table 1) which can reproduce the observed light curves. Models in brackets do not fulfil our criterion but are close. These models have been excluded for M-m.

Supernovae	in galaxy	Type	$v_z$	M-m	D[Mpc]	$E_{B-V}$	acceptable models
SN 1937C	IC 4182	Sm	326	28.3	$4.5 \pm 1$	0.10	N32,W7,DET2
SN 1970J	NGC 7619	dE	4019	34.0	$63 \pm 8$	0.01	DET2ENV2/4, (PDD3)
SN 1971G	NGC 4165	Sb	1703	32.8	$36 \pm 9$	0.04	M37, M36, W7, N32
SN 1972E	NGC 5253	I	407	28.0	$4.0 \pm 0.6$	0.04	M35,N21,M36 (HeD12 <sup>2</sup> )
SN 1972J	NGC 7634	SBO	3374	33.6	$52 \pm 8$	0.01	W7,M36/37,N32,DET2
SN 1973N	NGC 7495	Sc	5126	34.2	$69 \pm 20$	0.08	N32, M36, W7, (HeD10/11)
SN 1974G	NGC 4414	Sc	715	31.2	$17.5 \pm 5$	0.0	N32,M36,W7,DET2 (HeD10/11)
SN 1975N	NGC 7723	SBO	1823	32.2	$28 \pm 7$	0.18:	PDD3/6/9/1a
SN 1981B	NGC 4536	Sb	1647	31.4	$19 \pm 4$	0.05	M35, N21
SN 1983G	NGC 4753	S	1126	31.4	$15 \pm 4$	0.29	N32, W7 (M36)
SN 1984A	NGC 4419	Ep	1187	31.1	$16 \pm 4$	0.14	DET2ENV2, PDD3/6)
SN 1986G	NGC 5128	I	530	28.1	$4.2 \pm 1.2$	0.83	W7, N32, (M37/8)
SN 1988U	AC 118 <sup>1</sup>	-	91480	40.8	$1440 \pm 250$	0.05	M36, W7, N32
SN 1989B	NGC 3627	Sb	726	29.7	$8.7 \pm 3$	0.45	M37, M36
SN 1990N	NGC 4639	Sb	971	31.5	$20 \pm 5$	0.05	DET2ENV2/4, PDD3/1a
SN 1990T	PGC 63925	Sa	11980	36.2	$180 \pm 30$	0.1	M37, M38
SN 1990Y	anonym.	E	11680	36.4	$195 \pm 45$	0.05	W7, N32, M36/37, PDD3/6/1c
SN 1990af	anonym.	E	14989	37.1	$265 \pm 85$	0.05	W7, N32, M36
SN 1991M	IC 1151	Sb	2188	33.10	$41 \pm 10$	0.12	M35, PDD3
SN 1991T	NGC 4527	Sb	1727	30.4	$12 \pm 2$	0.10	PDD3/6/1a. DET2ENV2
SN 1991bg	NGC 4374	dE	954	31.3	$18 \pm 5$	0.25	PDD5/1c
SN 1992G	NGC 3294	Sc	1592	32.4	$29 \pm 6$	0.05	M36, M35, PDD3, HeD10
SN 1992K	ESO269-G57 <del>8</del> Bb	Sb	2908	33.2	$43_{-8}^{+15}$	0.18	PDD5/1a,(M39, HeD2)
SN 1992bc	ESO-G9	S	5960	34.6	$83 \pm 10$	0.04	PDD6/3/1c
SN 1992bo	ESO-G57	S	5662	34.5	$79 \pm 10$	0.03	PDD8
SN 1994D	NGC 4526	S0	487	31.1	$16 \pm 2$	0.00	M36, (W7, N32)

<sup>1</sup> the host galaxy is member of the cluster 118

<sup>2</sup> can be ruled because spectra indicate Si at higher velocities

## 7. Distance determinations, $H_0$ and $q_0$

The large absolute brightness of SNe Ia makes them very attractive candidates to determine extragalactic distances and the cosmological constants. The use of SNe Ia is based on the assumption that their absolute brightness is known. Unfortunately, SNe Ia are not standard candles, but their individual brightness in V may differ by several magnitudes. To overcome this problem, several groups have developed methods to allow for a sorting out of subluminous supernovae on basis of spectral peculiarities (Fisher et al. 1995) or by using correlations between the shape of the blue or visual light curves and the apparent magnitude (Hamuy et al. 1995; Ries, Press & Kirshner 1995). Both approaches allow for the use of SNe Ia or

a subset as standard or quasi-standard candles. The first approach has the advantage that the measurements can be corrected for interstellar reddening because a small variation of the intrinsic colors can be assumed for this subgroup (Miller and Branch, 1994). Unfortunately, it crucially depends on the homogeneity hypothesis for 'normal' bright SNe Ia both in terms of the brightness and the intrinsic color. Therefore, the criterion for disregarding observations must be very strict. In general, the Oklahoma group finds values for  $H_0$  of about 50 to 60  $km/Mpc\ sec$  with some preference towards the first value (e.g. Branch & Miller 1993, Miller & Branch 1990,1993; but see Fisher et al. 1995). Recently, a second approach has been used by two groups based on observational data and statistical analyses of 13 light curves mainly measured by the CTIO-group (Hamuy et al. 1995). The connections between the post-maximum decline in B (Phillips et al. 1993) or the shapes of the visual light curves (Riess et al. 1995) and the absolute brightness at maximum light have been investigated, respectively. Empirical relations have been found that allow for an excellent representation of the observational properties. The relation between the absolute brightness and the light curve shapes can be described by a one parameter family within an accuracy of  $0.21^m$  over the entire range of brightnesses observed, even without any correction for interstellar reddening (Riess et al. 1995). This makes SNe Ia 'quasi'-standard candles. Both groups derive  $H_0$  to be 65 and 67 within a one sigma error of 5 and 7, respectively (Hamuy et al. 1995, Riess et al. 1995).

The biggest advantage of purely empirical methods is their straightforward applicability and their independence from any physical assumption concerning explosion mechanisms. One of the disadvantages of empirical methods is their reliance on the accuracy of secondary distance indicators both for calibration purposes and for testing the relations. For a few cases, the period-luminosity relations of  $\delta$ -Cep stars has been used but, in general, the less accurate surface brightness fluctuation for galaxies have been used. For illustration of possible problems, several modern P(L) relations for  $\delta$ -Cep stars are given in Fig. 25. They show a spread of about  $0.5^m$ . Whether it is related to metallicity effects, mixing of stars pulsating in the first overtone and fundamental mode or based on systematic, observational errors calls for further investigations. Another disadvantage is the sensitivity to selection effects. Based on a larger sample of 35 light curves, the uniqueness of the relation between absolute brightness and shape of light curves has been questioned at the level of  $\approx 0.5^m$  (Hamuy et al. 1995b). Another problem may be that a correction for the interstellar reddening is not yet taken into account in the latter methods. Reddening corrections will be included in the near future because, apparent from a larger set of well-observed SN Ia, there also exists a strong relation between the intrinsic color and the absolute brightness (Riess & Kirshner, private communication). From the theoretical point of view, the intrinsic color and the brightness must be expected to depend on details such as the metallicity of the progenitor, mixing processes etc. because of the strong influence of metallicity on U and B, but, we cannot rule out the existence of a strong relation between intrinsic bright-

ness and color. A related problem is the k-correction which must be applied for distant SNe Ia at  $z \geq 0.025$ . Here, the intrinsic blue and UV wavelength ranges are shifted into the V filter range of the observer. Both from the observations (Hamuy et al. 1993a) and our models (sect. 3) it is clear that the k-correction in V varies significantly even for ‘normal’ SNe Ia.

A different, independent way to determine distances is the use of models (MH94) or of theoretical relations such as Arnett’s law (Arnett et al. 1985) to obtain the intrinsic brightness. Theoretical approaches do not rely on secondary distance scales although they can be tested by those (see next section), and they overcome most of the problems mentioned above. However, various uncertainties should be kept in mind, in particular, reliance on the assumption of SN Ia being standard candles (see sect. 2 and 3).

Our method is based on fitting observations of individual SNe Ia. Both the interstellar reddening and k-correction are consistent because the overall spectral energy distribution is given by the model. Doing this, we can determine a parameter range which reproduces the observed monochromatic light curves (and spectra) or which cannot be excluded from the observations. Consequently, this provides a measure for the allowed ranges of distance for the host galaxy and hence values H for the Hubble constant. These individual values are shown in Figure 26. The error bars for H reflect the uncertainties in the distance determination arising from model variations, observational uncertainties, and extinction corrections (Table 3). Our procedure does not rely on the assumption of a particular model or even mechanism because we have shown (e.g. sect. 3, HKM93, KMH93) that the intrinsic brightness is related to some other observable quantities almost independently from the scenario.

The individual values H for the Hubble constant  $H_O$  show a wide variation in our sample ranging from 30 to  $127 \text{ km s}^{-1} \text{ Mpc}^{-1}$ . The spread is caused by nearby SNe Ia with  $v_O \leq 1000 \text{ km/s}$  which, in several cases, are inconsistent with the uncertainty range of mean value  $\overline{H}$ . The scatter of the individual H values for more distant supernovae ( $v_O > 1000 \text{ km/s}$ ) is consistent within the statistical error of the mean Hubble constant  $\overline{H}$  and with a common value for  $H_O$ . We note that  $\overline{H}$  hardly depends on the exclusion of close supernovae. Both facts imply that all supernovae with  $v_O \leq 1000 \text{ km/s}$  are not yet in the Hubble flow and that peculiar, random motions dominate the local velocity field. The remaining systematic deviation is comparable with the dipole-field in the velocity v found by COBE (Stevens, Scott & Silk 1993) and the orientation of our residual values agrees roughly with the COBE results. Unfortunately, our sample of high quality data is too small ( $\approx 10$ ) to provide a reliable determination of the size of the dipole field, but, as a tendency, it seems somewhat smaller than implied by COBE. We estimate the uncertainty by, in quadrature, the sum over all distant supernovae of the statistical (table 4) and systematic errors. Based on the comparison between detailed NLTE and LC calculations (see section 2), we find  $H_O$  to be  $67.0 \pm 9 \text{ km s}^{-1} \text{ Mpc}^{-1}$  within a  $2 \sigma$  error. Alternatively, we can determine the error if we define the  $2 \sigma$  range



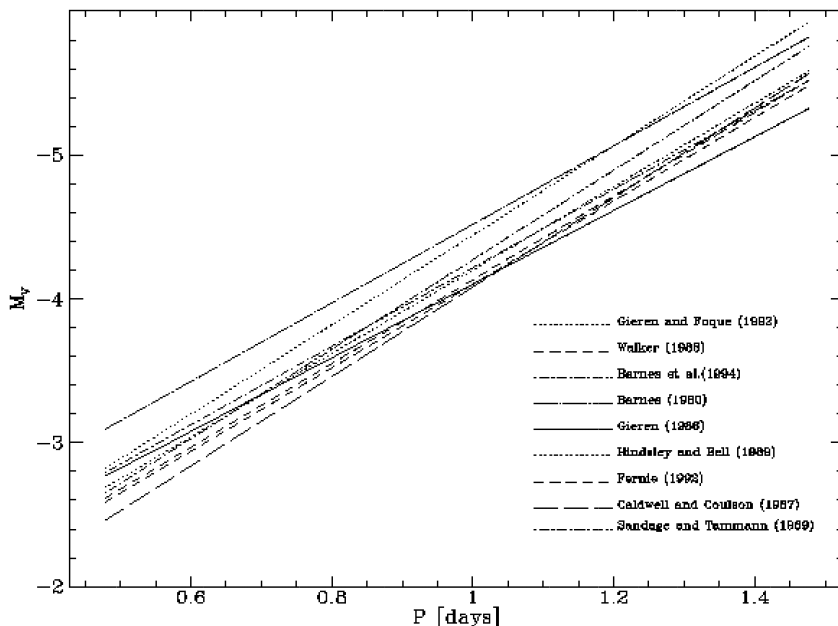


Figure 25: Period luminosity relations of  $\delta$ -Cep stars as given by various authors. The spread of up to  $0.5^m$  translates into a distance change of 25 %.

such that 95 % of our supernovae are within this range. If we assume that the individual errors are Gaussian, we get the same error range as given above. It must be remembered that the errors are non-Gaussian, but the consistency between the two different error estimates implies that our error range is realistic. Our new value of  $H_0$  is in good agreement with our previous estimate of  $66 \pm 10 \text{ km/s/Mpc}$  that was based on a smaller group of observations (50 %) and a subset (30 %) of models (MH94). Note that our value of  $H_0$  is hardly effected by possible problems with the six supernovae observed at Asiago because their small statistical weight (due to the large error bars) and the fact that the corresponding values are close to  $H_0$ . Recently, it was suggested that  $H_0$  may be as small as  $30 \text{ km sec}^{-1} \text{ Mpc}^{-1}$  on large scales (Bartlett et al 1995). From our analysis, this suggestion must be excluded, at least for scales smaller than 200 Mpc. In our sample with  $z \leq 0.3$ ,  $\Delta H_0 / \delta v$  is about  $1 \cdot 10^{-4} [\text{Mpc}^{-1}]$  which is consistent with no deviation from a linear Hubble-relation within the statistical errors (Table 4).

Finally, we want to stress that our value for the Hubble constant agrees well with that indicated by SNe II based on the Baade-Wesselink method for SNe II. Based on sophisticated atmospheres, which take the dilution of the radiation field by Thomson scattering properly into account,  $H_0$  was determined to be  $65 \pm 12$  (Höfllich 1990, 1991) and  $73 \pm 7 \text{ km/secMpc}$  (Schmidt et al. 1994) with  $1 \sigma$  errors.

Up to now, Euclidean space was assumed. Undoubtedly, this provides a very good description up to cosmological redshifts of  $z \leq 0.1$ . In light of the very distant supernova 1988U at  $z \approx 0.31$ , it is tempting to constrain the value of the deceleration parameter  $q_0$ . If we assume a Robert-Walker metric and set the cosmological

Table 4: Arithmetic mean  $\bar{H}$  of the individual values  $H$  for Hubble constant  $H_0$  based on  $n$  galaxies (column 8) with expansion velocities larger than  $v_0$  (column 1). Column 3 gives the standard deviation  $2\sigma_{Gauss}$  of  $H$ , if a Gaussian distribution is assumed (see text).  $\Delta H_0$  is the mean distance between  $H$  and  $\bar{H}$  and  $\Delta H_1$  denotes the maximum distance between the error ranges of  $H$  and  $\bar{H}$ . If  $\bar{H}$  lies within the uncertainty range of  $H$ ,  $\Delta H_1$  is zero. In columns 6 and 7,  $\delta H_0/\delta v$  and its standard deviation are given for  $z \leq 0.1$ . The values of the Hubble constants and the velocities are given in km/sec Mpc and km/sec.

$v_0$	$\bar{H}$	$2\sigma_{Gauss}$	$\Delta H_0$	$\Delta H_1$	$\delta H_0/\delta v$	$\sigma(\delta H_0/\delta v)$	$n$
5000.	67.0	4.	5.0	0.	-6.E-5	8.E-5	9
1000.	65.7	5.	7.5	0.	-2.E-5	1.1E-4	20
0.	67.6	7.	13.	20.	-8.0E-5	2.0E-4	26

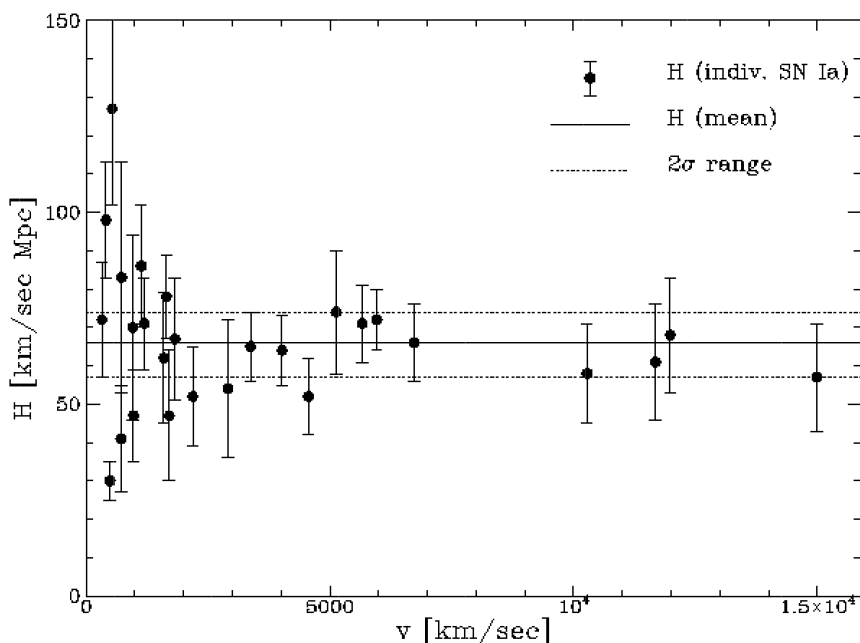


Figure 26: Hubble values  $H$  are shown based on individual distances (see Table 3). SN1988U at  $v=91500$  km/sec gives  $H = 64 \pm 10$  [km/sec Mpc].

constant to zero, the relation between the distance modulus, the Hubble constant, and  $q_0$  can be approximated by

$$m - M \approx 25 - 5\log(H_0) + 5\log(cz) + 1.086(1 - q_0)z \quad (7)$$

for  $z \leq 1.5$  (e.g. Weinberg 1972). Formally,  $q_0$  can be determined independently from the value of  $H_0$  because only flux ratios are measured by  $q_0$ . The uncertainties in the measurements enter by the probability functions of the individual measurements. However, the same errors enter the determination of  $q_0$  and  $H_0$ . To get a conservative estimate, we assume that the errors in  $H_0$  and in the individual distance of the high red shift supernova are additive. Using our value for  $H_0$ , SN1988U at  $z=0.31$  (Norgaard-Nielsen et al. 1989) and our distances from Table 3, we get  $q_0 = 0.7 \pm 0.5$ .

## 8. Discussion and Conclusions

To cover the entire set of scenarios for SNe Ia, Helium detonations of low-mass white dwarfs are presented, discussed in some detail, and included in our study with parameters close to those suggested by Woosley and Weaver (1994). Both bright and subluminous SNe Ia can be produced by Helium detonations ranging from  $V = -18.5^m$  to  $-19.7^m$ . By fine tuning the mass of the WD and mass of the helium layer atop, Helium detonations may be able to produce LCs somewhat dimmer by up to one magnitude if we use our  $V(M_{Ni})$  relation (Fig. 8). The lower limit is given by the critical amount of He to be burned in order to trigger a central detonation in carbon. The models follow the normal pattern previously found for other models—namely, the absolute brightness in V at maximum light is rather insensitive to the model as long as the mass of  $^{56}\text{Ni}$  exceeds  $\approx 0.4M_{\odot}$ . Helium detonations tend to be only marginally dimmer ( $\approx 0.1^m$ ) compared to the other scenarios. The differences to WW94 may be a consequence of differences in the opacities. In our calculations, the temperature dependence of the opacities has been taken into account, whereas WW94 assumed the opacities to be independent of chemistry, density, and temperature (see sect. 2). The distinguishing features of Helium detonations are blue maxima both for normal and subluminous supernovae, a rapid increase of the luminosity caused by  $^{56}\text{Ni}$  heating, followed by a phase of slow rise to maximum light and a fast post-maximum decline. The fast decline is caused by the rapid increase of the escape probability of gamma photons originating in the outer  $^{56}\text{Ni}$  and the fast decline rate of  $^{56}\text{Ni}$ .

The different explosion scenarios can generally be distinguished based on differences in the slopes of the early light curves and the photospheric expansion velocities. For all models with a  $^{56}\text{Ni}$  production  $\geq 0.4M_{\odot}$ ,  $M_V$  ranges from  $-19.1$  to  $-19.7^m$ . The peak brightness strongly declines with  $^{56}\text{Ni}$  for  $\leq 0.4M_{\odot}$  of  $^{56}\text{Ni}$ . As a general tendency, the post-maximum declines are related to  $M_V$ , but there is a significant spread in the decline rate among models with similar brightness. For all models but the Helium detonations, the colors become very red for small  $M_{Ni}$ .

The change of the apparent light curves due to the cosmological expansion has been discussed. Overall, LCs become dimmer with increasing red shift  $z$  because the energy is spread over a wider frequency range. The shapes of the light curves are significantly altered. In particular, the post maximum decline in the optical wavelength bands becomes steeper and the ratio between maximum light and the radioactive tail increases with  $z$ .

We find that a further  $z$ -correction is crucial for the interstellar reddening if  $z \geq 0.1$ . If a local extinction law is applied, estimates for the extinction become systematically wrong by up to a factor of two, depending on the red shift of the absorbing cloud. Even reddening as little as  $E_{B-V} = 0.05^m$  in a host galaxy at  $z=0.3$  translates into an error of about 10% in distance.

We presented a quantitative method for fitting data to models based on Wiener filtering (Rybicki and Press, 1995). The reconstruction technique is applied to the standard deviation from the theoretical LC to overcome problems with measurements distributed unevenly in time. The direct reconstruction of the light curves would have to deal with strongly variable correlation lengths. Our ansatz is equivalent to the assumption that the correlation length of the LC is given by the theoretical model to be fitted. By minimizing the error, the time of the explosion, the distance, and the reddening correction can be determined. Sadly, we find that the result of all these efforts agree pretty well with our previous fits based on ‘eye-balling’.

Observed monochromatic light curves of 27 SNe Ia are compared with theoretical light curves. According to our results, normal bright, fast Type Ia supernovae (e.g., SN 1971G, SN 1994D) with rise times up to 15 days (17 days) for the blue (visual) light curve can be explained by delayed detonation with different densities  $\rho_{tr}$  for the transition from a deflagration to a detonation. For PDDs, the density  $\rho_{tr}$  stands for the density at which the detonation starts after the first pulsation. Typically,  $\rho_{tr}$  is about  $2.5 \cdot 10^7 \text{ g/ccm}$ . Central densities of the initial WDs range from  $2.2$  to  $3.5 \cdot 10^9 \text{ g/ccm}$ . As a tendency, models at the lower end of this range tend to give somewhat better fits. This may be explained by a high accretion rate, some variation in the chemical composition or by an additional trigger mechanism for the explosion (a little He atop?). We note that the classical deflagration W7 (Nomoto et al. 1984) provides similar good fits in several cases because its structure resembles some of the delayed detonation models.

The “standard” explosion models are unable, however, to reproduce rise times to blue (visual) maximum longer than 15 days (16 days), provided the progenitor is a C/O white dwarf of about  $1.2$  to  $1.4 M_{\odot}$  (KMH92). In fact, slow rising and declining light curves have been observed (e.g., SN 1990N, SN 1991T) which require models with an envelope of typically  $0.2$  to  $0.4 M_{\odot}$ . The envelope can be produced during a strong pulsation or during the merging of two white dwarfs. The lower value should not be regarded as a physical limit, because it is likely that a continuous transition from models with and without an envelope exists. Note that a unique feature of this class of “non-standard” models is very high photospheric expansion velocities ( $v_{ph} \approx 16,000 \text{ km/s}$ ) at about maximum light, which drop rapidly to an almost constant value between  $9000$  and  $12,000 \text{ km/s}$ . This “plateau” in  $v_{ph}$  lasts for 1 to 2 weeks depending on the envelope mass (KMH93). In fact, there is some evidence for the plateau in  $v_{ph}$  from the Doppler shift of lines of SNe Ia which show a slow pre-maximum rise and post-maximum decline and for which spectra have been obtained (e.g., SN 1984A, SN 1990N) (MH94).

Strongly subluminous supernovae (SN1991bg, SN1992K, SN1992bc) can be explained within the framework of pulsating delayed detonation models with a low transition density. In particular, the models become systematically redder and the post-maximum decline becomes steeper with decreasing brightness (Table 2) in agreement with observations. However, we do not get unique relations between

these different quantities. The evolution of the photospheric expansion velocity  $v_{ph}$  (HKW95) and, in particular, its steady decline, is consistent with observations. We must also note that we need a rather high intrinsic reddening for SN1992K and SN1991bg. Whether this can be explained by selective line blanketing, dust formation, or foreground clouds, or a combined effect is under investigation. The latter possibility must be regarded as unlikely, because, at later phases, the colors of these two supernovae are close to those of bright SNe Ia. Note that some of the ‘classical’ delayed detonation models (M312, M39) also produce strongly subluminal LCs, but these do not fit any of the measurements.

Our Helium detonation models are rather unsuccessful in reproducing observations, mainly due to the rather steep post-maximum declines for normal bright supernovae. For strongly subluminal supernovae, the blue color at maximum light and the strong IR-maximum are both in contradiction to the observations. Further problems may arise for late time spectra because, for subluminal models, a large fraction of the entire  $^{56}\text{Ni}$  expands at rather high velocities. Quantitatively, multi-dimensional effects may alter the LCs mainly due to a higher escape probability for photons compared to the one-dimensional models. To test this, multi-dimensional radiation transport must be coupled with expansion opacities. Simple remapping of a 3-D structure would probably miss the main effect. However, the basic features of the LCs and spectra (sect. 2 & 3) are not expected to change because they are inherent to the outer  $^{56}\text{Ni}$ . In fact, the amount of nuclear He-burning is expected to be even larger in order to trigger the central C/O-detonation because the compression wave may be less focused compared to the 1-D case.

Our findings with respect to the explosion scenario can be concluded as follows. Models with masses close to the Chandrasekhar limit provide the best agreement with the observations. Delayed-detonation and deflagration models similar to W7 and pulsation or merging scenarios are required. We also have to emphasize that the current models are parameterized. A more realistic treatment, e.g. of the burning front, may quantitatively change the parameter range of successful models. We do not expect qualitative changes on the large scale structures of SNe Ia because of the time scales.

We found some evidence for a relation between the type of the explosion and of the host galaxy. In elliptical galaxies, SN Ia with shell-like structures are highly favored. These may be understood within the pulsating and merging scenarios. Because ellipticals consist on low mass stars only, this may provide a hint to the progenitor evolution; however, a larger sample of observations is needed to confirm this trend.

Based on our light curves, we have also determined the individual distances of the parent galaxies of the analyzed SNe Ia. Our method does not rely on secondary distance indicators and allows for a consistent treatment of interstellar reddening and the interstellar redshift. The advantages of a consistent inclusion of information from the spectra has been demonstrated for SN1990Y and SN1988U. The advantages are obvious if the data sets are rather sparse as can be expected for

distant SNe Ia. We find  $H_O$  to be  $67 \pm 9 \text{ km/secMpc}$  within a 95 % confidence level. This value agrees well with our previous analysis based on a subset of observations and models ( $66 \pm 10 \text{ km Mpc}^{-1} \text{ sec}^{-1}$ , MH94) and is consistent with the result of Shigeyama et al. (1992) which is based on W7 only. A strong variation of the local value can be ruled out at least on scales below 200 Mpc. From SN1988U, the deceleration parameter  $q_O$  is  $0.7 \pm 0.5$ . More and more distant supernovae are required to provide better limits. These measurements are currently under way by the Berkeley collaboration (Perlmutter et al. 1995), or may be provided as a by-product of deep sky surveys for galaxies if designed accordingly.

We want to mention some other determinations of  $H_O$  which are based on independent, purely statistical methods and primary distance indicators. The agreement with the value given above may indicate that, at least for SN Ia, the values obtained by methods which do not treat SNe Ia as standard candles are converging to similar values of  $H_O$ . Recently, Hamuy et al. (1995) found  $65 \pm 5$ , Riess et al. (1995) give  $67 \pm 5$ , and Fisher et al. (1995) get a value of  $60 \pm 10 \text{ km/Mpcsec}$ . From our models, both the empirical relations between the  $M_V/dM(15)$  like-relations and the ansatz to deselect subluminous supernovae seems to be justified, but we expect a dispersion of  $\approx 20\%$  for individual supernovae.

Note that, at maximum light in V, our models predict bolometric corrections  $BC = M_{bol} - M_V$  between  $-0.05^m$  to  $0.4^m$ <sup>1</sup>. Much larger values previously reported in literature ( $BC(SN 1981B) = 0.57^m$  and  $BC(SN 1992A) = 0.74^m$  at and five days after maximum light, respectively, Nugent et al. 1995a) have been corrected recently by  $\approx -0.5^m$  (Baron 1995, private communication). Since BC is a critical issue for the determination of  $H_O$  from models, we include a more detailed discussion in the appendix.

A comparison of our estimates for  $m_V - M_V$  with those determined from  $\delta$ -Cep stars of the host galaxies provides an additional test for the reliance of our models and, in particular, the monochromatic fluxes. From HST observations of  $\delta$ -Cep stars in IC4182, NGC5253, and NGC4536, distance moduli have been found to be  $28.47 \pm 0.08$ ,  $28.10 \pm 0.07$ , and  $31.17 \pm 0.20$  mag, respectively (Friedman et al. 1994; Sandage et al. 1994; Tammann 1995) which compare well with our estimates of  $28.3 \pm 0.25$ ,  $28.0 \pm 0.15$ , and  $31.4 \pm 0.21$  mag, respectively (see Table 3; Höflich et al. 1993b, Müller & Höflich 1994).

Finally, we have to bring up several open questions which are currently under investigation.

Some well observed SNe Ia show spectral peculiarities. Firstly, strong iron lines are observed in premaximum spectra of SN1991T (Filippenko al., 1992a) which may favor helium detonations rather than delayed detonations. However, both the very long rise time and the slow decline are in contradiction with helium detonation models and a significant amount of radioactive  $^{56}\text{Co}$  and  $^{56}\text{Ni}$  in the outer layers can

---

<sup>1</sup> e.g.  $BC(PDD5) = 0.4^m$ ,  $BC(W7, N32) = 0.2^m$ ,  $BC(DET2ENV2) = 0.1^m$ ,  $BC(M35) = -0.03^m$ ,  $BC(M36) = -0.05^m$

be excluded from late time spectra because the Fe and Co lines indicate velocities  $\leq 10,000 \text{ km/sec}$  (Spyromillo et al., 1992) without any evidence for  $^{56}\text{Co}$  moving at high velocities ( $\approx 14,000 \dots 17,000 \text{ km/sec}$ ). Note that, at late times, only the local energy deposition due to the  $\beta^+$  decay contributes to the light curve and, then, both the inner and the outer  $^{56}\text{Co}$  should contribute to the luminosity according to their mass ratio. A detailed study based on NLTE-model atmospheres is needed, to test whether the iron lines can be understood as a consequence of ionization equilibria or by an enhanced metallicity in the progenitor (Höflich et al. 1995c). Secondly, there is some evidence for Helium in SN1994D (Cumming, 1994ab) but, evidently, no enrichment of iron group elements as in SN1991T (H95). The He in SN1994D may be accumulated from the surrounding accretion disk. Alternatively, both helium and very little  $^{56}\text{Ni}$  in SN1994D and some  $^{56}\text{Ni}$  in SN1991T may be explained as following within the scenarios for white dwarfs close to the Chandrasekhar limit: If the accretion rate drops below the critical rate needed for steady burning, a little Helium can be accumulated atop the outer layers (e.g.  $0.01 M_{\odot}$ ). Close to the Chandrasekhar limit, the central density is very sensitive to the mass. Even this small increase in mass will cause a contraction and may trigger a deflagration wave starting in the center, or the Helium may detonate and this may trigger a deflagration rather a detonation in the center. We note, that neither of these scenarios would affect the determination of  $H_0$  because a little additional energy hardly increases the brightness and even classical helium detonations are comparably bright.

A second complex of open questions is related to the very red color observed in SN1991bg and SN1992K. Whether this can be understood by selective line blocking or dust formation is currently under investigation.

*Acknowledgement:* PAH would like to thank R.P. Kirshner and his group, and R. Hix for many useful discussions and S. Woosley for valuable comments during the Texas meeting in Munich. We also thank K. Nomoto for supplying his explosion model W7 in machine readable form. Special thanks go to J.C Wheeler for carefully reading the manuscript and valuable comments and to F.K. Thielemann for providing his marvelous network and many discussions and, last but not least, Al Cameron for his support including the computer equipment. We also want to thank the referee D. Branch, E.Müller and B. Press for useful discussions. We also want to thank G. Avrett, H. Uitenbroek and B. Kurucz for helpful discussions on the bolometric correction and the solar spectrum. This work has been supported by grant Ho1177/2-1 from the Deutsche Forschungsgemeinschaft.

### Appendix: Remark on Bolometric Corrections

Following the usual nomenclature, we define the bolometric correction BC as

$$BC = M_{bol} - M_V. \quad (A1)$$

We note that the quantity BC does not depend on the wavelength, but the use of the V band allows for transformation of the bolometric luminosity into the absolute brightness by relations given in literature (e.g. Lang 1980).

In light of recent discussions in literature on the correct size of BC at maximum light in V (Nugent et al. 1995b, Branch, private communication), it may be useful to investigate possible systematic uncertainties of our models which typically give values between 0. and  $0.2^m$  for normal bright supernovae.

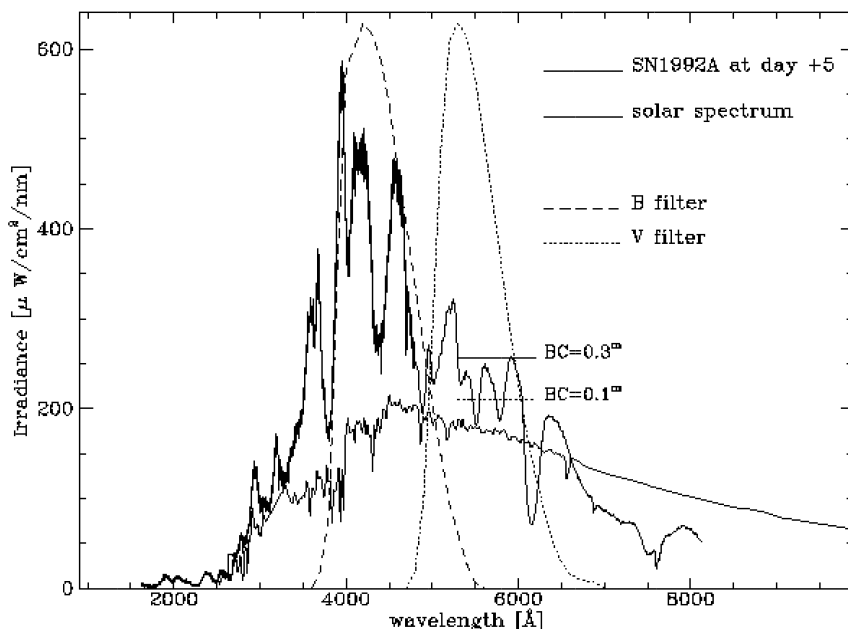


Figure A1: Comparison of the solar flux distribution (thin line, Kohl, Parkinson & Kurucz 1992, Neckel & Labs 1984, Labs & Neckel 1970, White 1977, Avrett 1992) with the observations of SN1992A at about 5 days past maximum light (thick line, Kirshner et al. 1993). Both spectra are normalized to the bolometric irradiance of the sun measured in  $\mu W/cm^2/nm$ . In addition, the B and V filter functions are given according to Bessell (1990). The horizontal lines at about 5500 Å give the mean flux level in V which would be required for BC of  $0.1^m$  (dots) and  $0.30^m$  (dashed dotted, new value of Nugent 1995 (private communication) based on spectral fits (Nugent et al. 1995b)).

Based on our NLTE-analysis of the blue SN1994D (H95) with  $BC \approx 0.^m$ , Branch (private communication) concluded that we may 'waste' UV flux and systematically underestimate BC. Admittedly, our calculated UV flux is rather uncertain due to the approximate treatment of line blanketing and scattering, etc.,



although we include several effects which, generally, are omitted (Kirshner et al. 1993, Harkness et al. 1995, Baron et al. 1995) – namely the fact that diffusion time scales at the photosphere are comparable to the expansion time scales. However, despite these uncertainties, strong limits on the systematic errors can be derived from the energy conservation. At maximum light, the UV flux is smaller than  $\approx 20\%$  of the total flux in all models. This implies a strict upper limit of  $0.20^m$  for the error in BC, if we assume that the entire UV flux is converted into optical photons. To provide a larger BC, flux from the U and B bands has to be converted. This happens soon after maximum light because line blanketing is rapidly increasing in U and B. Consistent with the observations of SNe Ia, the color indices become redder with time and our predicted BC increases to 0.1 to  $0.5^m$  on time scales of one to two weeks depending on the model. Note that, from the observations, a strong change of BC must be expected because the bolometric, B and V light curves do not peak at the same time. Consequently, the use of BC is very error-prone when it comes to the determination of absolute fluxes at maximum light. In contrast, using  $M_V$  and fitting the entire LC provides a robust procedure to determine absolute fluxes (e.g. in V) because it relies on the known total energy release by radioactive decay and the well measurable shape of the LC.

Another estimate of the correct value of BC can be obtained directly from observations. Some pre-maximum IUE observations are available for SN1990N and SN1981B, and very accurate HST measurements are available for SN1992A at about 5 days after the B maximum (Kirshner et al. 1993, Nugent et al. 1995a). The observed spectrum of SN1992A is given in comparison to the observed solar spectrum in Fig. A1. Both spectra are normalized to the same bolometric luminosity. Therefore, a comparison of the flux in the V band provides BC. In other wavelength bands (e.g. B), the difference between the fluxes is given by the sum of BC and the intrinsic color indices (e.g. B-V) compared to the solar values. For the normalization of the spectrum of SN1992A, we assume that the IR-flux of SN1992A becomes small above  $1 \mu m$ . The corresponding uncertainty in BC is  $\approx 0.1^m$ . We note that, historically, the bolometric corrections are normalized to a G2V star but, nowadays,  $BC(Sun) = -0.07^m$  of the sun is used as reference point (Lang 1980, Avrett 1992). Only 8 % of the solar radiation is emitted in the UV and the solar flux peaks in the optical wavelength band (Fig. A1). Therefore, BC is negative for all main sequence stars. The UV flux of SN1992A is comparable to the sun, making it impossible to produce a large BC correction by redistributing UV photons. Instead, the flux in B is increased at the expense of the IR-flux producing the blue color index in SN Ia ( $B - V(SN1992A) = 0.1^m$  vs.  $B - V(Sun) = 0.67^m$ ). Physically, the reduced IR-flux in supernovae is caused by the smaller free-free emission as a consequence of the lower densities at the photosphere. Apparently, the gain in V is very moderate. Most of the flux difference in the B band can be attributed to the differences in the intrinsic colors. Both for the B and V band, BC is between 0. and  $0.2^m$  which is consistent with our models for 'normal' bright supernovae.

Note that the new value of BC  $0.30^m$  for SN1992A (Nugent 1995, private com-

munication) seems to be slightly too high compared to the observations (Fig. A1). However, this discrepancy should not be overvalued because, for atmospheres, small inconsistencies in the physical and numerical approximations will cause errors in the radial distribution of the density, abundances, and temperature, which enter quadratically the absolute flux (H95).

## References

- Arnett W. D. 1969, *Ap. Space Sci.*, 5, 280
- Arnett W.D. 1982, in *Supernovae*, ed. (Dordrecht: D.Reidel), p.221
- Arnett W.D., Branch D., Wheeler J.C. 1985, *Nature*, 314, 337
- Avrett G. 1992, in *Proceedings of the Workshop on the Solar Electromagnetic Radiation Study for Solar Cycle 22*, ed. R.F. Donnelly (NOAA ERL: Springfield), p.20
- Barbon R., Ciatti F., Rosino L. 1973, *A&A*, 29, 57
- Barbon R., Benetti S., Cappellaro E., Rosino L., Turatto M. 1990, *A&A*, 237, 79
- Barbon R., Cappellaro E., Turatto M. 1989a, *A&AS*, 81, 421
- Barbon R., Iijima T., Rosino L. 1989b, *A&A*, 220, 83
- Barnes T. G. I., Moffett T.J., Gieren W.P. 1994, *ApJ*, 405L, 51
- Barnes T. G. I. 1980, *JAtSc*, 37, 2002
- Baron E., Hausschild P.H., Branch D., Austin S., Garnavich P., Ann H.B., Wagner R.M., Filippenko A.V., Matheson T., Liebert J. 1995, *ApJ*, 441, 170
- Bartlett J.G., Blanchard A., Silk J., Turner M.S. 1995, *Nature*, submitted and astro-ph/9407061
- Benz W., Thielemann F, Hills J.G. 1989, *ApJ*, 342, 986
- Bessell M. 1990,, *PASP*, 102, 1181
- Branch D. 1981, *ApJ* , 248, 1076
- Branch D., Tammann G.A 1992, in *Type Ia Supernovae as Standard Candles*, ed. S. van den Bergh (Berlin/Heidelberg/New York : Springer Press, Ann.Reviews), p.267
- Branch D. 1993, *ApJ*, 405, L5
- Burstein D., Heiles C. 1984, *ApJS*, 54, 33
- Cadonau R., Leibundgut B. 1990, *A&AS*, 82, 145
- Caldwell J. A. R., Coulson I. M. 1987, *AJ*, 93, 1090
- Canal R. 1995, in *Proc. of Les Houches Session LIX*, ed. J. Audouze, S. Bludman, R. Mochovitch, J. Zinn-Jutin (Paris: Elsevier Science Publishers), in press
- Capaccioli M., Cappellaro E., Della Valle M., D'Onofrio M., Rosino L., Turatto M. 1990, *ApJ*, 350, 110
- Challis P. 1994, private communication
- Ciatti F., Rosino L. 1978, *A&AS*, 34, 387
- Collela P., Woodward P.R. 1984, *J. Comp. Phys.*, 54, 174
- Cowan J.J., Thielemann F.-K., Truran J. W. 1991, *Phys. Rep.*, 208, 267
- Cristiani S., Cappellaro, E., Turatto M., Bergeron J., Bues I., Buson L., Danziger J., Di Serego-Alighieri S., Duerbeck H.W., Heydari-Malayeri M., Krautter J., Schmutz W., Schulte-Ladbeck R.E. 1992, *A&A*, 259, 63
- Cumming R.J. 1994a, *IAU-circular*, 5953
- Cumming R.J. 1994b, *IAU-circular*, 5951

- Della Valle M., Panagia N. 1992, AJ, 104, 696
- Dominik C., Höflich P., Khokhlov A. 1995, ApJ, in preparation
- Fernie J. D. 1992, AJ, 103, 1647
- Filippenko A.V., Richmond M.W., Matheson T., Shields J.C., Burbidge E.M., Cohen R.D., Dickinson M., Malkan M.A., Nelson B., Pietz J., Schlegel D., Schmeer P., Spinrad H., Steidel C.C., Tran H.D., Wren W. 1992a, ApJ, 384, L15
- Filippenko A.V., Richmond M.W., Branch D., Gaskell C.M., Herbst W., Ford C.H., Treffers R.R., Matheson T., Ho L.C., Dey A., Sargent W.L., Small T.A., van Breugel W.J.M. 1992b, AJ, 104, 1543
- Fisher A., Branch D., Höflich P., Khokhlov A., Wheeler J.C. 1995, ApJ Let, in press
- Ford C.H., Baker M.L., Filippenko A.V., Treffers R.R., Paik Y., Benson P.J. 1993, AJ, 106, 1101
- Freedman, W. L.; Madore, B. F.; Mould, J. R.; Hill, R.; Ferrarese, L.; Kennicutt, R. C.; Saha, A.; Stetson, P. B.; Graham, J. A.; Ford, H.; Hoessel, J. G.; Huchra, J.; Hughes, S. M.; Illingworth, G. D. 1994, Nature, 371, 75
- Frogel J.A., Gregory B., Kawara K., Laney D., Phillips M.M., Terndrup D., Vrba F., Whitford, A.E. 1987, ApJ, 315, L129
- Gieren W.P., Barnes T. G. I., Moffett T.J. 1993, ApJ, 418, 135
- Gieren W.P., Foque P. 1992, AJ, 106, 734
- Gieren W.P. 1986, ApJ, 306, 25
- Hachisu I., Eriguchi Y., Nomoto K. 1986a, ApJ, 308, 161
- Hachisu I., Eriguchi Y., Nomoto K. 1986b, A&A, 168, 130
- Hamuy M. et al. 1993a, AJ, 106, 2392
- Hamuy M. et al. 1993b, PASP, 105, 787
- Hamuy M. et al. 1994, AJ, 108, 2226
- Hamuy M., Phillips M.M., Maza J., Suntzeff N.B., Schommer R.A., Aviles A. 1995, AJ, in press
- Hamuy M., Höflich P., Khokhlov A., Wheeler J.C. 1995b, ApJ Let, in preparation
- Hansen C. J., Wheeler J. C. 1969, Ap. Space Sci., 3, 464
- Hindsley R.R., Bell R.A. 1989, ApJ, 341, 1004
- Höflich, P. 1990, *Habilitation Thesis, Ludwig Maximilians Univ.* (München: published as MPA-90 563)
- Höflich P., Khokhlov, A., Müller, E. 1992, A&A, 259, 549
- Höflich P. 1991, in *Supernovae*, ed. S. Woosley (New York: Springer-Press), p.415
- Höflich P., Khokhlov A., Müller E. 1991a, A&A, 259, 243
- Höflich P., Khokhlov A., Müller E. 1991b, A&A, 248, L7
- Höflich P., Müller E. & Khokhlov A. 1993, A&A, 268, 570
- Höflich P., Müller, E., Khokhlov A., 1993b, in *Supernovae and Supernovae Remnants*, ed. D. McCray, Z. Wang & Z. Li (Xiang: Cambridge University Press), in press
- Höflich P., Khokhlov A., Wheeler J.C. 1995, ApJ, in, press
- Höflich P. 1995, ApJ, 443, 533

- Höflich P., Müller E., Khokhlov A., Wheeler C.J. 1995b, in 17<sup>th</sup> *Texas Symposium on Relativistic Astrophysics*, ed. Trümper (Munich: Springer), p.in press
- Höflich P., Khokhlov A., Nomoto K., Thielmann F.K., Wheeler C.J. 1995c, in *Type Ia Supernovae*, ed. Barcellona (R. Canal, J. Isern, P. Ruiz-Lapuente: Kluver), Amsterdam  
in preparation
- Hook I., McMahon R. 1991, IAU-Circular, 5218
- Hoyle F., Fowler W. A. 1960, Ap. J., 132, 565
- Iben I.Jr., Tutukov A.V. 1984, ApJS, 54, 335
- Iijima T., Turatto M., Cappellaro E. 1992, IAU-Circular, 5456 & 5458
- Ivanova I. N., Imshennik V. S., Chechetkin V. M. 1974, ApSS, 31, 497
- Jöeveer M. 1982, Afz, 18, 574
- Karp A.H., Lasher G., Chan K.L., Salpeter E.E. 1977, ApJ, 214, 161
- Kogoshvili K. 1986/1993, in *Selected Astronomical Catalogs CD Vol. I*, ed. L.E. Brotzman & S.E. Gessner (Greenbelt: National Space Science Data Center), p.
- Khokhlov A. 1991a, A&A, 245, 114
- Khokhlov A. 1991b, A&A, 245, L25
- Khokhlov A., Müller E., Höflich P. 1992, A&A, 253, L9
- Khokhlov A., Müller E., Höflich, P. 1993, A&A, 270, 223
- Kirshner, R. P. et al. 1993, ApJ, 415, 589
- Knude J.K. 1977, ApJ.Let., 18, 115
- Kohl J.L., Parkinson W.H., Kurucz B.L. 1992, *Center and Limb Solar Spectrum in High Spectral Resolution from 225.2 nm to 319.6 nm* (National Bureau of Standards: Boulder)
- Kosai, J. 1992, IAU-circular, 5452,
- Labs D., Neckel H. 1970, Sol. Phys., 15, 79
- Lamla L. 1982, in *Landold Börnstein, New Series B 2a*, ed. (: ), p.54
- Lang C. 1980, *Astrophysical formulae* (Springer Press: Berlin/Heidelberg/New York)
- Leibundgut B., Kirshner R.P., Filippenko A.V., Shields J.C., Foltz C.B., Phillips M.M., Sonneborn G. 1991, ApJ, 371, L23
- Leibundgut B. et al. 1993, AJ, 105, 301
- Livne E. 1990, ApJ, 354, 53
- Livne E., Glasner A.S. 1990, ApJ, 361, L244
- Marvin H., Perlmutter S. 1989, IAU-Circular, 4727
- Maza J., Hamuy M., Phillips M.M., Suntzeff N.B., Ayiles R. 1994, ApJ, 424, L107
- Miller D.L., Branch D. 1990, AJ, 103, 379
- Mihalas D. 1978, *Stellar atmospheres* (Freeman: San Francisco)
- Miller D.L., Branch D. 1990, AJ, 100, 530
- Müller E., Höflich P. 1991, in *SN1987A and Other Supernovae*, ed. I.J. Danziger and K. Kjär (Garching: ESO), p.379
- Müller E., Höflich P. 1994, A&A, 281, 51

- Neckel H., Labs D. 1984, *Solar Phys.*, 90, 205
- Nomoto K., Sugimoto S., & Neo S. 1976, *ApSS*, 39, L37
- Nomoto K., Sugimoto D. 1977, *PASJ*, 29, 765
- Nomoto K. 1980, in *IAU-Sym. 93*, ed. D. Sugimoto, D.Q. Lamb & D. Schramm (Dordrecht: Reidel), p.295
- Nomoto K. 1982, *ApJ*, 253, 798
- Nomoto K., Thielemann F.-K., Yokoi K. 1984, *ApJ*, 286, 644
- Nomoto K., Yamaoka H., Shigeyama T., Iwamoto K. 1995, in *Supernovae and Supernova Remnants*, ed. R. A. McCray, Z. Wang & Z. Li (Cambridge: Cambridge University Press), in press
- Norgaard-Nielsen H.U., Hansen L., Henning E.J., Salamanca A.A., Ellis R.S., Warwick, J.C. 1989, *Nature*, 339, 523
- Nugent P., Baron E., Hauschild P., Branch D. 1995a, *ApJ Lett.*, 441, L33
- Nugent P., Branch D., Baron E., Fisher A., Vanghan T. 1995b, *Phys. Rev. Lett.*, submitted
- Paczynski B. 1985, in *in: Cataclysmic Variables and Low-Mass X-Ray Binaries*, ed. D.Q. Lamb, J. Patterson (Reidel: Dordrecht), p. 1
- Pennypacker C. et al. 1991, *IAUC*, 5207
- Perlmutter C. et al. 1995, *ApJ Lett.*, 440, 95
- Phillips M. M. 1993, *ApJ*, 413, L108
- Phillips M.M., Phillips A.C., Heathcote S.R., Blanco V.M., Geisler D., Hamilton D., Suntzeff N.B., Jablonski F.J., Steiner J.E., Cowley A.P., Schmidtke P., Wyckopf S., Hutchings J.B., Tonry J., Strauss M.A., Thorstensen J.R., Honey W., Maza J., Ruiz M.T., Landolt A.U., Uomoto A., Rich R.M., Grindlay J.E., Cohn H., Smith H.A., Lutz J.H., Lavery R.J., Saha A. 1987, *PASP*, 90, 592
- Pskovskii Yu.P. 1970, *Astron. Zh.*, 47, 994
- Pskovskii Yu.P. 1977, *Sov. Astr.*, 21, 675
- Riess A.G., Press W.H., Kirshner R.P. 1995, *ApJ*, 438, L17
- Ruiz-Lapuente P., Jeffery D., Challis P.M., Filippenko A.V., Kirshner R.P., Ho L.H., Schmidt B.P., Sanchez F., Canal R. 1993, *Nature*, 365, 728
- Rybicki G.B., Press W.H. 1995, *Phys.Rev.Lett.*, in press
- Sandage A., Tammann G.A. 1969, *ApJ*, 157, 683
- Sandage A., Tammann G.A. 1993, *ApJ*, 415, 1
- Sandage A, Saha A., Panagia N., Panagia N., Macchetto F.D. 1992, *ApJ*, 401, L7
- Sandage A, Saha A., Tammann G.A., Labhardt L., Schwengler H., Panagia N., Macchetto F.D. 1994, *ApJ*, 423, L13
- Schaller G., Schaerer D., Meynet G., Maeder A. 1992, *A&A Suppl*, 96, 269
- Schmidt B.P. et al. 1994, *ApJ*, 432, 42
- Shigeyama T., Nomoto K., Yamaoka H., Thielemann F.K. 1992, *ApJ*, 386, L13
- Spyromilio J., Meikle W.P.S., Allen D.A., Graham J.R. 1992, *MNRAS*, 258, 53p
- Stevens D., Scott D., Silk J. 1993, *PhRvL*, 71, 20S
- Thielemann F.-K., Nomoto K., Hashimoto M. 1994, in *Supernovae*, ed. Les Houches (S. Bludman R., Mochkovitch J., Zinn-Justin: Elsevier), p.Amsterdam

- Thielemann F.-K., Arnould M., Truran J.W. 1987, in *Advances in Nuclear Astrophysics*, ed. E. Vangioni-Flam (Editions frontières: Gif sur Yvette), p.525
- Tsvetkov, D.Yu 1994, *Astron.L.*, 20, 374
- Van den Bergh S., Pazder J. 1992, *ApJ*, 390, 34
- Walker, A.R. 1988, *PASP*, 100, 949
- Webbink R.F. 1984, *ApJ*, 277, 355
- Weinberg, S. 1972, *Gravitation and Cosmology: Principles and Applications of the General Theory of Relativity* (New York: John Wiley & Sons)
- Wells L.A. + 45 coauthors 1994, *AJ*, 108, 2235
- Wheeler J. C., Harkness R .P. 1990, *Rep. Prog. Phys.*, 53, 1467
- Wheeler J. C., Harkness R .P., Khokhlov A., Höflich P. 1995, *Phys. Rep.*, in press
- White O.R. 1977, *The SSolar Output and its Variation* (Colorado Associated Univ. Press: Boulder)
- Woosley S.E., Weaver T.A. 1986, *ARAA*, 24,
- Woosley S. E. & Weaver , T. A. 1995, in *Proc. of Les Houches Session LIX*, ed. J. Audouze, S. Bludman, R. Mochovitch, J. Zinn-Jutin (Paris: Elsevier Science Publishers), in press
- Woosley S. E. & Weaver, T. A. 1994, *Ap. J.*, 423, 371
- Woosley S. E., Weaver T.A., Taam R.E. 1980, in *in: Type I Supernovae*, ed. C.Wheeler (Austin: U.Texas), p.96
- Yamaoka H., Nomoto K., Shigeyama T., Thielemann F. 1992, *ApJ*, 393, 55